Microbiome–host systems interactions: Protective effects of propionate upon the blood–brain barrier

Lesley Hoyles[1]*, Tom Snelling[1], Umm-Kulthum Umlai[1], Jeremy K. Nicholson[1], Simon R. Carding[2, 3], Robert C. Glen[1, 4] & Simon McArthur[5]*

[1]Division of Integrative Systems Medicine and Digestive Disease, Department of Surgery and Cancer, Imperial College London, UK

[2]Norwich Medical School, University of East Anglia, UK

[3]The Gut Health and Food Safety Research Programme, The Quadram Institute, Norwich Research Park, Norwich, UK

[4]Centre for Molecular Informatics, Department of Chemistry, University of Cambridge, Cambridge, UK

[5]Institute of Dentistry, Barts & the London School of Medicine & Dentistry, Blizard Institute, Queen Mary University of London, London, UK

***Corresponding authors:** Lesley Hoyles, lesley.hoyles11@imperial.ac.uk; Simon McArthur, s.mcarthur@qmul.ac.uk

Running title: Propionate affects the blood–brain barrier

Abbreviations: ADHD, attention-deficit hyperactivity disorder; ASD, autism spectrum disorder; BBB, blood–brain barrier; CNS, central nervous system; FFAR, free fatty acid receptor; KEGG, Kyoto Encyclopaedia of Genes and Genomes; GO, Gene Ontology;

LPS, lipopolysaccharide; SCFA, short-chain fatty acid; SPIA, Signalling Pathway Impact Analysis.

Abstract

Background: Gut microbiota composition and function are symbiotically linked with host health, and altered in metabolic, inflammatory and neurodegenerative disorders. Three recognized mechanisms exist by which the microbiome influences the gut–brain axis: modification of autonomic/sensorimotor connections, immune activation, and neuroendocrine pathway regulation. We hypothesized interactions between circulating gut-derived microbial metabolites and the blood–brain barrier (BBB) also contribute to the gut–brain axis. Propionate, produced from dietary substrates by colonic bacteria, stimulates intestinal gluconeogenesis and is associated with reduced stress behaviours, but its potential endocrine role has not been addressed.

Results: After demonstrating expression of the propionate receptor FFAR3 on human brain endothelium, we examined the impact of a physiologically relevant propionate concentration (1 μM) on BBB properties *in vitro*. Propionate inhibited pathways associated with non-specific microbial infections via a CD14-dependent mechanism, suppressed expression of LRP-1 and protected the BBB from oxidative stress via NRF2 (NFE2L2) signaling.

Conclusions: Together, these results suggest gut-derived microbial metabolites interact with the BBB, representing a fourth facet of the gut–brain axis that warrants further attention.

Background

The human body plays host to, and exists in symbiosis with, a significant number of microbial communities, including those of the skin, oral and vaginal mucosae and, most prominently, the gut [1]. This relationship extends beyond simple commensalism to represent a major regulatory influence in health and disease, with changes in abundance of members of the faecal microbiota having been associated with numerous pathologies, including diabetes, hepatic diseases, inflammatory bowel disease, viral infections and neurodegenerative disorders [2–8]. Metagenomic studies have revealed reductions in microbial gene richness and changes in functional capabilities of the faecal microbiota to be signatures of obesity, liver disease and type II diabetes, and that these can be modified by dietary interventions [9,10]. The gut microbiome harbours 150 times more genes than the human genome, significantly increasing the repertoire of functional genes available to the host and contributing to the harvesting of energy from food [11].

The primary form of communication within the gut microbe–human super-system is metabolic, but our understanding of the details of the cross-signalling pathways involved is limited. It is clear, however, that gut-derived microbial metabolites and products such as lipopolysaccharide (LPS) can influence human health both in the intestine and systemically [12,13], with reported effects ranging from mediation of xenobiotic toxicity [14], through modification of the risk of preterm birth [15] to induction of epigenetic programming in multiple host tissues [16,17]. A major aspect of microbe–host systems-level communication that is receiving increased attention is the influence the gut microbiota exerts upon the central nervous system (CNS), the so-called ‘gut–brain axis’ [18].

The existence of gut–brain communication is supported by a number of animal and human studies, although the underlying mechanisms are not always well defined. Behavioural analysis of antibiotic-treated or germ-free rodents reveals alterations in both stress responsiveness [19] and anxiety [20–22], although in germ-free models these findings are complicated by the life-long absence of gut microbes and possible consequent developmental alterations. Nonetheless, gut-microbe-depleted animals have been shown to exhibit changes in serotonergic and glutamatergic neuronal signalling [20] and expression of brain-derived neurotrophic factor (BDNF) within the limbic system [22,23], providing a molecular correlate for behavioural changes.

Links between the gut microbiota and brain function have been identified in studies of humans with autism spectrum disorders (ASD) and attention-deficit hyperactivity disorder (ADHD). Altered microbial profiles have been identified in children with ASD [24–26], and oral treatment of autistic children with the non-absorbed, broad-spectrum antibiotic vancomycin – effectively suppressing the gut microbiota – led to a regression in autistic behavioural characteristics that was reversed upon antibiotic discontinuation [27]. Similarly, a small-scale intervention study has suggested not only a link between lower counts of faecal *Bifidobacterium* species at six months and increased incidence of ADHD at 13 years, but also that early probiotic treatment lessens the risk of ADHD development [28].

A number of unresolved questions remain as to the mechanism(s) of communication between the gut microbiota and the brain, but three major pathways have been proposed: direct modification of vagal or sympathetic sensorimotor function [29],

inflammatory/immune activity [30] and neuroendocrine crosstalk [31]. While research in this field has focussed most heavily on direct neural modulation and inflammatory signalling, the potential role of circulating gut microbe-derived metabolites has been relatively underexplored. Communication with and across the blood–brain barrier (BBB), the primary interface between the circulation and the CNS, may therefore represent a significant mechanism allowing the gut microbiota to influence brain function.

There is accumulating evidence that the gut microbiota can affect the integrity of the BBB, with both broad-spectrum-antibiotic-treated and germ-free mice exhibiting considerably enhanced barrier permeability and dysregulation of inter-endothelial cell tight junctions [32,33]. Importantly, these impairments can be reversed upon conventionalisation. The mechanism(s) by which gut microbes exert their influence are unclear, but changes to brain chemistry induced by alteration of the gut microbiota can occur independently of vagal or sympathetic neural pathways and in the absence of any immune response, strongly suggesting at least a contributory role for soluble gut-derived microbial metabolites [22].

In particular, data highlight a potential role for short-chain fatty acids (SCFAs) as key microbial mediators in the gut–brain axis. SCFAs are principally produced by the fermentation of complex plant-based polysaccharides by gut bacteria and are potent bioactive molecules; stimulating colonic blood flow and upper-gut motility, influencing H_2O and NaCl uptake, providing energy for colonocytes, enhancing satiety and positively influencing metabolic health in obese and diabetic individuals [34–36]. Of the SCFAs, acetate is produced in the greatest quantity as a result of fermentation in

the large intestine, followed by propionate and butyrate [37]. Over 95 % of SCFAs produced are absorbed within the colon with virtually none appearing in the urine or faeces [35,38]. However, all three metabolites are detectable in the peripheral blood of healthy individuals (http://www.hmdb.ca: acetate, 22–42 μM; propionate, 0.9–1.2 μM; butyrate, 0.3–1.5 μM). SCFAs activate members of the free fatty acid receptor (FFAR) family of G protein coupled receptors; acetate, propionate and butyrate have affinity in the low millimolar to high micromolar range for FFAR2; propionate and butyrate have mid to low micromolar affinity for FFAR3 [39].

The majority of studies looking at the role of SCFAs in the gut–brain axis have focused on butyrate [40], with relatively few investigating propionate despite its similar plasma concentration and receptor affinity. Propionate is a highly potent FFAR3 agonist for its size (agonist activity GTPγS pEC_{50} (E_{max}) 3.9-5.7(100%)) and has close to optimal ligand efficiency ($-\Delta G$=1.26 kcal mol^{-1} $atom^{-1}$) for this receptor [41]. While propionate has been shown to stimulate intestinal gluconeogenesis through direct stimulation of enteric–CNS pathways [42], and increased intestinal propionate has been associated with reduced stress behaviours [43] and reward pathway activity [44] in mice and humans, respectively, its potential role as an endocrine mediator in the gut–brain axis has not been addressed. Given the presence of FFAR3 on endothelial cells [45], we hypothesised that propionate targeting of the endothelium of the BBB would represent an additional facet of the gut–brain axis. We used a systems approach to test this proposal, performing an unbiased study of the transcriptomic effects of exposure to physiological levels of propionate upon the BBB, modelled by the immortalised human cerebromicrovascular endothelial cell line hCMEC/D3, accompanied by *in vitro* validation of identified pathway responses.

Results

Microarray analyses

Following initial confirmation of the expression of FFAR3 in human brain endothelium (**Fig. 1a**) and on hCMEC/D3 cells (**Fig. 1b**), we investigated the effect of exposure of hCMEC/D3 monolayers to 1 μM propionate for 24 h. Such treatment had a significant (P_{FDR} < 0.1) effect on the expression of 1136 genes: 553 upregulated, 583 downregulated (**Fig. 1c**). Initially, we used SPIA with all the significantly differentially expressed genes to identify KEGG signalling pathways inhibited and activated in the presence of propionate. Protein processing in the endoplasmic reticulum and RNA transport were activated upon exposure of cells to propionate, which was unsurprising given gene expression had been induced. A number of pathways associated with non-specific microbial infections (Gram-negative bacteria, viral) were inhibited by propionate (**Fig. 1d**), as were the cytosolic DNA-sensing pathway (upregulated by pathogen DNA during microbial infections, triggering innate immune signalling [46]), the NFκB signalling pathway and the Toll-like receptor signalling pathway. Of the 19309 genes we examined on the array, 203 of the 224 genes known to be associated with the BBB were detected (**Supplementary Table 1**). Eleven of these were significantly differentially expressed, with the majority being associated with the inflammatory response.

Enrichr [47,48] was used to examine KEGG pathways significantly associated with the list of significantly differentially expressed genes. All 1136 significantly differentially expressed genes mapped to Enrichr. As with SPIA, the genes were associated with

KEGG pathways implicated in non-specific microbial infections, and RNA- and endoplasmic reticulum-associated processes (**Fig. 1e**).

WikiPathways analysis (Enrichr) of all the significantly differentially expressed genes highlighted responses to oxidative stress being associated with propionate treatment (not shown). Closer examination of the data demonstrated this was linked to NRF2 (NFE2L2) signaling, with the significantly upregulated genes closely associated with oxidative stress responses (**Fig. 1f**).

Pathway validation

Transcriptomic analysis identified two particular clusters of pathways as being regulated by propionate treatment: those involved in the non-specific inflammatory response to microbial products (**Fig. 1d, e**) and those involved in the response to oxidative stress (**Fig. 1f**). We, therefore, sought to validate these responses in an *in vitro* model of the BBB.

TLR-specific pathway

Inhibition of the TLR-specific pathway by propionate suggests this metabolite may have a protective role against exposure of the BBB to bacterial lipopolysaccharide (LPS), derived from the cell walls of Gram-negative bacteria. In accord with this hypothesis, exposure of hCMEC/D3 monolayers for 12 h to propionate at physiological concentrations (1 μM) was able to significantly attenuate the permeabilising effects of exposure to *Escherichia coli* O111:B4 LPS (subsequent 12 h stimulation, 50 ng/ml), measured both through paracellular permeability to a 70 kDa FITC-conjugated dextran tracer (**Fig. 2a**) and trans-endothelial electrical resistance (**Fig. 2b**). To determine the

specificity of these effects for propionate, we investigated the actions of the closely related SCFAs acetate and butyrate. While physiologically relevant circulating concentrations of butyrate (1 μM) replicated the effects of propionate on both trans-endothelial electrical resistance and paracellular tracer permeability, this was not the case for acetate (65 μM) (**Fig. 2a-b**).

Circulating concentrations of propionate are approximately 1 μM at rest, but these may be expected to increase following consumption of, for example, a meal containing high levels of fermentable fibre [1], consequently we examined the effects of 10 μM and 100 μM propionate upon the response of hCMEC/D3 monolayers to LPS stimulation. Both LPS-induced deficits in trans-endothelial electrical resistance (**Suppl. Fig. 1a**) and paracellular tracer permeability (**Suppl. Fig. 1b**) were fully attenuated by higher doses of propionate, without any obvious further effects beyond those seen with 1 μM of the SCFA.

Although hCMEC/D3 cells are a widely used *in vitro* model of the BBB, they are not without limitations, particularly in terms of their higher inherent permeability when compared with other non-human model systems [49]. To ensure the validity of our findings using hCMEC/D3 cells, we repeated these experiments using primary human brain microvascular endothelial cells (HBMECs). As with hCMEC/D3 cells, exposure of HBMEC monolayers for 12 h to propionate (1 μM) significantly attenuated the permeabilising effects of LPS exposure (subsequent 12 h stimulation, 50 ng/ml), in terms of both paracellular permeability to a 70 kDa FITC-conjugated dextran tracer (**Suppl Fig. 2a**) and trans-endothelial electrical resistance (**Suppl Fig. 2b**). Given this

confirmation, subsequent experiments focused solely on the hCMEC/D3 cells as an *in vitro* BBB model.

Paracellular permeability and trans-endothelial electrical resistance are in large part dependent upon the integrity of inter-endothelial tight junctions [50], which are known to be disrupted following exposure to LPS [51]. We, therefore, examined the intracellular distribution of the key tight junction components occludin, claudin-5 and zona occludens-1 (ZO-1) following treatment with propionate and/or LPS. Exposure of hCMEC/D3 monolayers to propionate alone (1 μM, 24 h) had no noticeable effect on the intracellular distribution of any of the studied tight junction components, whereas treatment with LPS (50 ng/ml, 12 h) caused a marked disruption in the localisation of all three major tight junction molecules, characterised by a loss of peri-membrane immunoreactivity (**Fig. 2c**). Notably, these effects of LPS were substantially protected against by prior treatment for 12 h with 1 μM propionate.

LPS initiates a pro-inflammatory response through binding to Toll-like receptor 4, TLR4, in a complex with the accessory proteins CD14 and LY96 (MD2) [52]; we, therefore, examined expression of TLR4 signalling components as an explanation for the protective effects of propionate upon this pathway. While propionate treatment of hCMEC/D3 cells (1 μM, 24 h) had no significant effect upon expression of mRNA for TLR4 or LY96 (data not shown), such treatment significantly down-regulated expression of *CD14* mRNA (**Fig. 2d**), an effect replicated at the level of cell surface CD14 protein expression (**Fig. 2e, f**).

NFE2L2 (NRF2) signalling and protection from oxidative stress

Enrichr (WikiPathways) analysis indicated that exposure of hCMEC/D3 cells to propionate resulted in the regulation of a number of antioxidant systems. Of known human anti-oxidant genes [53], 58 were detected on the array. We had also identified an additional 6 genes via [54] (**Supplementary Table 2**). Searches of the genes associated with each of the individual pathways referenced in **Fig. 1f** strongly indicated these changes occurred downstream of the transcription factor nuclear factor, erythroid 2 like 2 – NFE2L2 (**Fig. 3a**). Supporting this analysis, exposure of hCMEC/D3 cells for 24 h to 1 μM propionate caused a marked translocation of NFE2L2 from the cytoplasm to the nucleus (**Fig. 3b**). Functional analysis of antioxidant pathway activity was assessed by monitoring reactive oxygen species production in hCMEC/D3 cells following exposure to the mitochondrial complex I inhibitor rotenone (2.5 μM, 2 h). Pre-exposure of cells to 1 μM propionate for 24 h significantly attenuated the rate of fluorescent tracer accumulation, indicative of reduced levels of intracellular reactive oxygen species (**Fig. 3c**).

Efflux transporter expression and activity

A key feature of the BBB is the expression of a wide array of efflux transporter proteins, which limit entry of numerous endogenous and xenobiotic agents to, and promote their export from, the brain. Amongst these, the proteins P-glycoprotein, BCRP and LRP-1 are prominent examples. We investigated the ability of propionate to both modify expression of these transporters and, in the case of the ABC transporter proteins P-glycoprotein and BCRP, serve as a direct inhibitor or substrate for the protein. Exposure of hCMEC/D3 monolayers to propionate at physiological levels (1 μM) for 24 h significantly suppressed expression of LRP-1 without modulating expression of either BCRP or P-glycoprotein (**Supplementary Fig. 1a, b**). Similarly, propionate had

neither a stimulatory nor inhibitory effect upon either BCRP or P-glycoprotein activity, at concentrations between 12 nM and 27 μM (**Supplementary Fig. 1c-f**).

Discussion

Considerable effort has gone into interrogating the gut–brain axis over recent years, with a steadily growing appreciation of the influence of the gut microbiota upon CNS function in health and disease. Mechanistic studies have identified three principal aspects to the gut–brain axis: modification of autonomic sensorimotor connections [29], immune activation [30], and regulation of neuroendocrine pathways [31], all of which incorporate a role for soluble gut-derived microbial agents, whether metabolic products or structural microbial components (e.g. LPS) themselves. In the current study, we identify a fourth facet to the gut–brain axis, namely the interactions between gut-derived microbial metabolites and the primary defensive structure of the brain, the BBB. In particular, we identify a beneficial, protective effect of the SCFA propionate upon the BBB, mitigating against deleterious inflammatory and oxidative stimuli.

If confirmed *in vivo*, our findings of protective effects of propionate upon BBB endothelial cells *in vitro* will add to the previously described beneficial actions of the SCFA upon a number of metabolic parameters. Propionate has been shown to improve glucose tolerance and insulin sensitivity, reduce high-density lipoprotein and increase serum triglyceride concentrations [35,55,56], all of which result in a more stable metabolic homeostasis. The effects of propionate upon the BBB that we describe in this study add to these pro-homeostatic actions, emphasising the contribution the SCFA plays to maintaining normal physiological function. Given that

296 the main source of circulating propionate in humans is the intestinal microbiota [57,58],
297 following fermentation of non-digestible carbohydrates by select bacterial species
298 (**Fig. 4**), propionate thus represents a paradigm of commensal, mutually beneficial
299 interactions between the host and microbiota. Moreover, consumption of food
300 containing non-digestible carbohydrates increases circulating propionate
301 concentrations approximately ten-fold [59,60], suggesting that the anti-inflammatory
302 effects of the SCFA upon the cerebrovascular endothelium may be another facet of
303 the known health benefits of high-fibre diets [61].

304

305 That BBB integrity is influenced by the gut microbiota and that SCFAs may play a role
306 in this process was recently emphasised in studies of germ-free *vs.* specific pathogen-
307 free mice, with germ-free animals exhibiting enhanced BBB permeability and disrupted
308 cerebral endothelial tight junctions [32]. These permeability defects were reversed fully
309 upon conventionalisation with a pathogen-free microbiota, and partially with
310 monocultures producing various SCFAs. Moreover, defective BBB integrity could be
311 ameliorated at least partially by extended oral administration of sodium butyrate. Our
312 findings thus cement SCFAs as a key group of gut-derived microbial mediators
313 modulating BBB function, and provide evidence emphasising a direct action through
314 the circulation. Propionate acts primarily through either of the two free fatty acid
315 receptors FFAR2 or FFAR3 [41], which although absent from neurones in the CNS
316 [62] have been identified in the cerebral endothelium [45], with FFAR3 confirmed
317 herein, indicating a possible mechanism of action. Although further study would be
318 required to prove it conclusively, our data suggest that FFAR3 may be the predominant
319 receptor type mediating the protective effects of SCFAs, as while the major ligands for
320 this receptor, propionate and butyrate, were both able to prevent a functional decline

in BBB integrity induced by LPS exposure, this was not the case for acetate, an SCFA with greater potency at FFAR2 [39]. Future work investigating the relative contributions of the two receptor types to BBB integrity will be informative.

Notably, and perhaps unsurprisingly, SCFAs cannot fully recapitulate the BBB-restoring effects of conventionalisation of germ-free animals, as revealed in the current work and previously [32,33]. It, therefore, seems likely that additional circulating gut-derived microbial mediators may contribute to the regulation of BBB function, and are thus highly deserving of future investigation. Given that upwards of 200 distinct microbial metabolites have been identified in the circulation of healthy individuals and animals [61,63], there is clearly great potential for intestinal dysbiosis and the resultant variation in metabolite levels to influence the BBB.

This may be highly relevant to the development of neurological disease, as variation in BBB function is increasingly recognised to impact on cognitive processes, although the mechanism(s) underlying this link are poorly understood. In particular, defects in BBB integrity have been linked with impaired memory [64] and linguistic [65] function, as well as with inferior performance on psychometric tests such as the mini mental state exam [66] and Oxford handicap scale [67]. Antibiotic-induced intestinal dysbiosis has been associated with similar cognitive deficits and with a reduction in circulating gut-derived microbial metabolites [33], but as yet whether the BBB plays a role in this connection has not been investigated. If this is the case, however, as the current study suggests, regulation of BBB function by microbe-derived mediators may be an important component in some of the emerging links between intestinal dysbiosis and pathologies as significant as depression [68], Parkinson's disease [69,70] and

Alzheimer's disease [71]. Notably, patients with early Parkinson's or Alzheimer's diseases have been shown to bear reduced levels of *Bacteroides* species within their faeces [71,72]. Given that *Bacteroides* spp. are important producers of SCFAs, including propionate [57], from complex carbohydrates (**Fig. 4**), this reduction may lead to a decline in circulating propionate and consequent vulnerability of the BBB, and, by extension, the brain in these major neurological conditions.

Modulatory effects of circulating gut-derived microbial metabolites upon the BBB may also be a component of the beneficial outcomes seen upon consumption of prebiotics or probiotics in a number of neurological conditions. For example, small-scale clinical trials have identified beneficial effects of probiotic drinks on cognitive ability in both Alzheimer's disease [73] and multiple sclerosis [74], conditions associated with reduced BBB integrity [75]. Similarly, oral administration of prebiotic oligosaccharides to mice significantly reduced anxiety and stress behaviours, effects that correlated with increases in caecal acetate, propionate and butyrate concentrations [43]. Whether such changes in caecal SCFA reflected plasma levels was not measured, but given that SCFAs can be transported across the gut epithelium [76,77] increases in circulating concentrations may be likely. That inflammation contributes to depression has become clearer over recent years [78], hence it is conceivable that the anti-inflammatory effects of propionate we describe may underlie at least part of the protective effects of prebiotic treatment, a proposal which, though speculative, is deserving of further study.

In summary, we reveal here a significant new aspect of the gut–brain axis, namely the modulatory effects of circulating gut-derived microbial metabolites upon the endothelium of the BBB. Given the critical gate-keeping role the BBB plays in

communication between the periphery and the brain parenchyma, our findings set the stage for future investigation of the influence the gut microbiota has on this structure, and the impact intestinal dysbiosis may have upon individual susceptibility to neurological and psychological diseases.

Materials & Methods

Human Tissue

Human post mortem samples were taken from the prefrontal cortex from non-neurologic controls; brains were retrieved from the UK Multiple Sclerosis Society tissue bank at Imperial College London, under ethical approval from the UK MRC Brain Bank Network (Ref. No. 08/MRE09/31+5). Brains were selected according to the following criteria: (i) availability of full clinical history, (ii) no evidence of cancer post mortem, and (iii) negligible atherosclerosis of cerebral vasculature. Tissue was fixed in 10% v/v buffered formalin and embedded in paraffin. From each paraffin block, 5 µm sections were cut and used for immunohistochemistry for FFAR3 using standard protocols [79], with a primary rabbit anti-FFAR3 polyclonal antibody (1:100; Stratech Scientific, Newmarket, UK), a horseradish peroxidase-conjugated goat anti-rabbit secondary antibody (1:300; Stratech Scientific, UK), and 2,3-diaminobenzidine and hydrogen peroxide as chromogens. Images were taken using a Leica DM5000 bright-field microscope equipped with a x40 oil immersion objective, and analysed using NIH ImageJ 1.51h (National Institutes of Health, USA).

Cerebromicrovascular cells

The human cerebromicrovascular endothelial cell line hCMEC/D3 was purchased from VHBio Ltd (Gateshead, UK), maintained and treated as described previously [79–81]. Cells were cultured to confluency in complete EGM-2 endothelial cell growth medium (Lonza, Basel, Switzerland), whereupon medium was replaced by EGM-2 without VEGF and cells were further cultured for a minimum of 4 days to enable intercellular tight junction formation prior to experimentation. Primary human cerebromicrovascular endothelial cells (HBMEC) were purchased from Sciencell

Research Laboratories (San Diego, CA, USA) and were maintained in ECM growth medium according to the supplier's recommendations. Cells were cultured to confluency in complete ECM (Sciencell Research Laboratories, USA), whereupon medium was replaced by EGM-2 without VEGF and cells were further cultured for a minimum of 4 days to enable intercellular tight junction formation prior to experimentation. For primary cultures, trans-endothelial electrical resistance was measured as described below, and experiments were only undertaken when this had reached approximately 200 $\Omega.cm^2$.

Microarrays

hCMEC/D3 cells were grown on 6-well plates coated with calf-skin collagen (Sigma-Aldrich, Gillingham, UK) to confluency as described above, further cultured for 4 days in EGM-2 medium without VEGF and exposed to propionate (1 μM, 24 h). Cells were collected into TRIzol (Thermo-Fisher Scientific, UK) and total RNA was extracted using a TRIzol Plus RNA purification kit (Thermo-Fisher Scientific, UK) and quantified using an ND-1000 Spectrophotometer (NanoDrop, Wilmington, USA).

Hybridization experiments were performed by Macrogen Inc. (Seoul, Korea) using Illumina HumanHT-12 v4.0 Expression BeadChips (Illumina Inc., San Diego, CA). RNA purity and integrity were evaluated using an ND-1000 Spectrophotometer (NanoDrop, USA) and an Agilent 2100 Bioanalyzer (Agilent Technologies, Palo Alto, USA). Total RNA was amplified and purified using TargetAmp-Nano Labelling Kit for Illumina Expression BeadChip (EPICENTRE, Madison, USA) to yield biotinylated cRNA according to the manufacturer's instructions. Briefly, 350 ng of total RNA was reverse-transcribed to cDNA using a T7 oligo(dT) primer. Second-strand cDNA was

synthesized, *in vitro*-transcribed, and labelled with biotin-NTP. After purification, the cDNA was quantified using the ND-1000 Spectrophotometer (NanoDrop, USA).

Labelled (750 ng) cDNA samples were hybridized to each beadchip for 17 h at 58 °C, according to the manufacturer's instructions. Detection of array signal was carried out using Amersham fluorolink streptavidin-Cy3 (GE Healthcare Bio-Sciences, Little Chalfont, UK) following the bead array manual. Arrays were scanned with an Illumina bead array reader confocal scanner according to the manufacturer's instructions. The quality of hybridization and overall chip performance were monitored by visual inspection of both internal quality control checks and the raw scanned data. Raw data were extracted using the software provided by the manufacturer (Illumina GenomeStudio v2011.1, Gene Expression Module v1.9.0).

Processing and analyses of array data

Raw data supplied by Macrogen were quality-checked, $\log_2$-transformed and loess-normalized (2 iterations) using affy [82]. Probes annotated as 'Bad' or 'No match' in illuminaHumanv4.db [83] were removed from the dataset (n = 13,631) [84]. After this filtering step, only probes with valid Entrez identifiers (n = 28,979) were retained for further analyses. Entrez identifiers were matched to official gene symbols using 'Homo_sapiens.gene_info', downloaded from https://www.ncbi.nlm.nih.gov/guide/genes-expression/ on 14 January 2017. Average gene expression values were used for identification of differentially expressed genes. Array data have been deposited in ArrayExpress under accession number E-MTAB-5686.

Signaling Pathway Impact Analysis (SPIA) was used to identify Kyoto Encyclopedia of Genes and Genomes (KEGG) pathways activated or inhibited in hCMEC/D3 cells exposed to propionate [85]. Enrichr [47,48] was used to confirm KEGG findings (with respect to pathways, not their activation/inhibition) and to perform Gene Ontology (GO)- and WikiPathways-based analyses.

In vitro barrier function assessments

Paracellular permeability and transendothelial electrical resistance were measured on 100 % confluent cultures polarised by growth on 24-well plate polyethylene terephthalate (PET) transwell inserts (surface area: 0.33 cm^2, pore size: 0.4 μm; Appleton Woods, UK) coated with calf-skin collagen and fibronectin (Sigma-Aldrich, UK). The permeability of endothelial cell monolayers to 70 kDa FITC-dextran (2 mg/ml) was measured as described previously [81,86,87]; data are presented as the contribution to the permeability barrier provided by endothelial cells, P_e, throughout. Transendothelial electrical resistance (TEER) measurements were performed using a Millicell ERS-2 Voltohmmeter (Millipore, Watford, UK) and were expressed as $\Omega.cm^2$. In all cases, values obtained from cell-free inserts similarly coated with collagen and fibronectin were subtracted from the total values. Briefly, cells were treated with propionate (1 μM) for 24 h prior to analysis of barrier function. In some cases, barrier integrity was tested by challenge with bacterial lipopolysaccharide (LPS). Confluent endothelial monolayers were treated with propionate (1 μM) for 12 h, whereupon LPS (*Escherichia coli* O111:B4; 50 ng/ml, comparable to circulating levels of LPS in human endotoxemia [88]) was added for a further 12 h, without wash-out. Barrier function characteristics were then interrogated as described above.

Efflux transporter assays

Activity of the major efflux transporters P-glycoprotein and BCRP [89] was determined through the use of commercially available assays (Solvo Biotechnology Inc., Budapest, Hungary), performed according to the manufacturer's instructions. Step-wise dose-response curves centred around reported physiological circulating concentrations of propionate [90] were constructed (n=2) and both activating and inhibitory effects of propionate upon transporter activity were analysed.

Flow cytometry analysis

hCMEC/D3 cells were labelled with APC-conjugated mouse monoclonal anti-CD14 (Thermo-Fisher Scientific, Paisley, UK), APC-conjugated mouse monoclonal anti-BCRP (BD Biosciences, Oxford, UK), FITC-conjugated mouse monoclonal LRP1 (BD Biosciences, UK), PE-conjugated mouse monoclonal anti-MDR1A (BD Biosciences, UK), unconjugated rabbit polyclonal antibody directed against FFAR3/GPR41 (Flarebio Biotech LLC, College Park, MD, USA) followed by incubation with an AF488-conjugated goat anti-rabbit secondary antibody (Thermo-Fisher Scientific, UK), or appropriate isotype controls (all BD Biosciences, UK) for analysis by flow cytometry. Briefly, hCMEC/D3 cells were treated for 24 h with propionate (1 μM), detached using 0.05 % trypsin and incubated with antibodies as described above. Immunofluorescence was analysed for 20,000 events per treatment using a BD FACSCanto II (BD Biosciences, UK) flow cytometer and data were analysed using FlowJo 8.0 software (Treestar Inc., CA, USA).

Immunofluorescence analysis

hCMEC/D3 cells were cultured on Lab-Tek™ Permanox™ 8-well chamber slides coated with calf-skin collagen (Sigma-Aldrich, UK), prior to immunostaining according to standard protocols [79,81] and using primary antibodies directed against Nrf2 (1:500, Novus Biologicals Ltd., Abingdon, UK), occludin (1:200, Thermo-Fisher Scientific, UK), claudin-5 (1:200, Thermo-Fisher Scientific, UK) and zona occludens-1 (ZO-1; 1:100, Thermo-Fisher Scientific, UK). Nuclei were counterstained with DAPI (Sigma-Aldrich, UK). Images were captured using an LSM880 confocal laser scanning microscope (Carl Zeiss Ltd., Cambridge, UK) fitted with 405 nm, 488 nm, and 561 nm lasers, and a 63x oil immersion objective lens (NA, 1.4 mm, working distance, 0.17 mm). Images were captured with ZEN imaging software (Carl Zeiss Ltd., UK) and analysed using ImageJ 1.51h (National Institutes of Health, USA).

Statistical analyses

Sample sizes were calculated to detect differences of 15 % or more with a power of 0.85 and α set at 5 %, calculations being informed by previously published data [79,81]. *In vitro* experimental data are expressed as mean ± SEM, with n=3 independent experiments performed in triplicate for all studies. In all cases, normality of distribution was established using the Shapiro–Wilkes test, followed by analysis with two-tailed Student's *t*-tests to compare two groups or, for multiple comparison analysis, 1- or 2-way ANOVA followed by Tukey's HSD *post hoc* test. Where data was not normally distributed, non-parametric analysis was performed using the Wilcoxon signed rank test. A P value of less than or equal to 5 % was considered significant. Differentially expressed genes were identified in microarray data using LIMMA [91]; P values were corrected for multiple testing using the Benjamini–Hochberg procedure

(False Discovery Rate); a *P* value of less than or equal to 10 % was considered significant in this case.

Declarations

Ethics approval and consent to participate

Not applicable

Consent for publication

Not applicable

Availability of data and material

Array data have been deposited in ArrayExpress under accession number E-MTAB-5686 (http://www.ebi.ac.uk/arrayexpress/experiments/E-MTAB-5686/)

Competing interests

The authors declare that they have no competing interests

Funding

This work was funded by Alzheimer's Research UK Pilot Grant no. ARUK-PPG2016B-6. This work used the computing resources of the UK MEDical BIOinformatics partnership – aggregation, integration, visualization and analysis of large, complex data (UK MED-BIO), which is supported by the Medical Research Council (grant number MR/L01632X/1). Human tissue samples and associated clinical and neuropathological data were supplied by the Multiple Sclerosis Society Tissue Bank,

549 funded by the Multiple Sclerosis Society of Great Britain and Northern Ireland,
550 registered charity 207495. LH is in receipt of an MRC Intermediate Research
551 Fellowship in Data Science (MR/L01632X/1, UK MED-BIO). TS received a bursary
552 from Imperial College London as part of the Undergraduate Research Opportunities
553 Programme.

554

555 *Authors' contributions*

556 LH and SM conceived the experiments; LH, TS, UU and SM performed experiments;
557 LH and SM analysed the data; LH and SM wrote the paper; JKN, SRC and RCG
558 provided valuable insight and advice throughout the project.

559

560 *Acknowledgements*

561 Not applicable

562

563 **References**

564

565 1. Nicholson JK, Holmes E, Kinross J, Burcelin R, Gibson G, Jia W, et al. Host-gut
566 microbiota metabolic interactions. Science. 2012;336:1262–7.

567 2. Forslund K, Hildebrand F, Nielsen T, Falony G, Le Chatelier E, Sunagawa S, et al.
568 Disentangling type 2 diabetes and metformin treatment signatures in the human gut
569 microbiota. Nature. 2015;528:262–6.

570 3. Ley RE, Bäckhed F, Turnbaugh P, Lozupone CA, Knight RD, Gordon JI. Obesity
571 alters gut microbial ecology. Proc. Natl. Acad. Sci. U. S. A. 2005;102:11070–5.

572 4. Manichanh C, Rigottier-Gois L, Bonnaud E, Gloux K, Pelletier E, Frangeul L, et al.
573 Reduced diversity of faecal microbiota in Crohn's disease revealed by a metagenomic
574 approach. Gut. 2006;55:205–11.

575 5. Turnbaugh PJ, Hamady M, Yatsunenko T, Cantarel BL, Duncan A, Ley RE, et al. A
576 core gut microbiome in obese and lean twins. Nature. 2009;457:480–4.

577 6. Qin N, Yang F, Li A, Prifti E, Chen Y, Shao L, et al. Alterations of the human gut
578 microbiome in liver cirrhosis. Nature. 2014;513:59–64.

579 7. Monaco CL, Gootenberg DB, Zhao G, Handley SA, Ghebremichael MS, Lim ES, et
580 al. Altered Virome and Bacterial Microbiome in Human Immunodeficiency Virus-
581 Associated Acquired Immunodeficiency Syndrome. Cell Host Microbe. 2016;19:311–
582 22.

583 8. Smith MI, Yatsunenko T, Manary MJ, Trehan I, Mkakosya R, Cheng J, et al. Gut
584 microbiomes of Malawian twin pairs discordant for kwashiorkor. Science.
585 2013;339:548–54.

586 9. Campbell SC, Wisniewski PJ, Noji M, McGuinness LR, Häggblom MM, Lightfoot
587 SA, et al. The Effect of Diet and Exercise on Intestinal Integrity and Microbial Diversity
588 in Mice. PLoS One. 2016;11:e0150502.

589 10. Shoaie S, Ghaffari P, Kovatcheva-Datchary P, Mardinoglu A, Sen P, Pujos-Guillot
590 E, et al. Quantifying Diet-Induced Metabolic Changes of the Human Gut Microbiome.
591 Cell Metab. 2015;22:320–31.

592 11. Zhu B, Wang X, Li L. Human gut microbiome: the second genome of human body.
593 Protein Cell. 2010;1:718–25.

594 12. Patterson E, Cryan JF, Fitzgerald GF, Ross RP, Dinan TG, Stanton C. Gut
595 microbiota, the pharmabiotics they produce and host health. Proc. Nutr. Soc.
596 2014;73:477–89.

597 13. Li M, Wang B, Zhang M, Rantalainen M, Wang S, Zhou H, et al. Symbiotic gut
598 microbes modulate human metabolic phenotypes. Proc. Natl. Acad. Sci.
599 2008;105:2117–22.

14. Zheng X, Zhao A, Xie G, Chi YY, Zhao L, Li H, et al. Melamine-induced renal toxicity is mediated by the gut microbiota. Sci. Transl. Med. 2013;5:172ra22.

15. Kindinger LM, MacIntyre DA, Lee YS, Marchesi JR, Smith A, McDonald JAK, et al. Relationship between vaginal microbial dysbiosis, inflammation, and pregnancy outcomes in cervical cerclage. Sci. Transl. Med. 2016;8:350ra102.

16. Bhat MI, Kapila R. Dietary metabolites derived from gut microbiota: critical modulators of epigenetic changes in mammals. Nutr. Rev. 2017;75:374–89.

17. Krautkramer KA, Rey FE, Denu JD. Chemical signaling between gut microbiota and host chromatin: What is your gut really saying? J. Biol. Chem. 2017;jbc.R116.761577.

18. Sherwin E, Rea K, Dinan TG, Cryan JF. A gut (microbiome) feeling about the brain. Curr. Opin. Gastroenterol. 2016;32:96–102.

19. Sudo N, Chida Y, Aiba Y, Sonoda J, Oyama N, Yu X-N, et al. Postnatal microbial colonization programs the hypothalamic-pituitary-adrenal system for stress response in mice. J. Physiol. 2004;558:263–75.

20. Neufeld KM, Kang N, Bienenstock J, Foster JA. Reduced anxiety-like behavior and central neurochemical change in germ-free mice. Neurogastroenterol. Motil. 2011;23:255–e119.

21. Heijtz RD, Wang S, Anuar F, Qian Y, Bjorkholm B, Samuelsson A, et al. Normal gut microbiota modulates brain development and behavior. Proc. Natl. Acad. Sci. 2011;108:3047–52.

22. Bercik P, Denou E, Collins J, Jackson W, Lu J, Jury J, et al. The intestinal microbiota affect central levels of brain-derived neurotropic factor and behavior in mice. Gastroenterology. 2011;141:599–609, 609.e1–3.

23. Hoban AE, Moloney RD, Golubeva AV, McVey Neufeld KA, O'Sullivan O, Patterson E, et al. Behavioural and neurochemical consequences of chronic gut microbiota depletion during adulthood in the rat. Neuroscience. 2016;339:463–77.

627 24. Finegold SM, Downes J, Summanen PH. Microbiology of regressive autism.
628 Anaerobe. 2012;18:260–2.

629 25. Finegold SM, Dowd SE, Gontcharova V, Liu C, Henley KE, Wolcott RD, et al.
630 Pyrosequencing study of fecal microflora of autistic and control children. Anaerobe.
631 2010;16:444–53.

632 26. Mezzelani A, Landini M, Facchiano F, Raggi ME, Villa L, Molteni M, et al.
633 Environment, dysbiosis, immunity and sex-specific susceptibility: A translational
634 hypothesis for regressive autism pathogenesis. Nutr. Neurosci. 2015;18:145–61.

635 27. Sandler RH, Finegold SM, Bolte ER, Buchanan CP, Maxwell AP, Vaisanen M-L,
636 et al. Short-Term Benefit From Oral Vancomycin Treatment of Regressive-Onset
637 Autism. J. Child Neurol. 2000;15:429–35.

638 28. Pärtty A, Kalliomäki M, Wacklin P, Salminen S, Isolauri E. A possible link between
639 early probiotic intervention and the risk of neuropsychiatric disorders later in childhood:
640 a randomized trial. Pediatr. Res. 2015;77:823–8.

641 29. Forsythe P, Bienenstock J, Kunze WA. Vagal pathways for microbiome-brain-gut
642 axis communication. Adv. Exp. Med. Biol. 2014;817:115–33.

643 30. Powell N, Walker MM, Talley NJ. The mucosal immune system: master regulator
644 of bidirectional gut–brain communications. Nat. Rev. Gastroenterol. Hepatol.
645 2017;14:143–59.

646 31. Cani PD, Knauf C. How gut microbes talk to organs: The role of endocrine and
647 nervous routes. Mol. Metab. Elsevier; 2016;5:743–52.

648 32. Braniste V, Al-Asmakh M, Kowal C, Anuar F, Abbaspour A, Tóth M, et al. The gut
649 microbiota influences blood-brain barrier permeability in mice. Sci. Transl. Med.
650 2014;6:263ra158.

651 33. Fröhlich EE, Farzi A, Mayerhofer R, Reichmann F, Jačan A, Wagner B, et al.
652 Cognitive Impairment by Antibiotic-Induced Gut Dysbiosis: Analysis of Gut Microbiota-
653 Brain Communication. Brain. Behav. Immun. 2016;56:140–55.

654 34. Roediger WE. Role of anaerobic bacteria in the metabolic welfare of the colonic
655 mucosa in man. Gut. 1980;21:793–8.

656 35. Salminen S, Bouley C, Boutron-Ruault MC, Cummings JH, Franck A, Gibson GR,
657 et al. Functional food science and gastrointestinal physiology and function. Br. J. Nutr.
658 1998;80 Suppl 1:S147–71.

659 36. Frost G, Sleeth ML, Sahuri-Arisoylu M, Lizarbe B, Cerdan S, Brody L, et al. The
660 short-chain fatty acid acetate reduces appetite via a central homeostatic mechanism.
661 Nat. Commun. Nature Publishing Group; 2014;5:672–9.

662 37. Cummings JH, Pomare EW, Branch WJ, Naylor CP, Macfarlane GT. Short chain
663 fatty acids in human large intestine, portal, hepatic and venous blood. Gut.
664 1987;28:1221–7.

665 38. Topping DL, Clifton PM. Short-chain fatty acids and human colonic function: roles
666 of resistant starch and nonstarch polysaccharides. Physiol. Rev. 2001;81:1031–64.

667 39. Alexander SP, Davenport AP, Kelly E, Marrion N, Peters JA, Benson HE, et al.
668 The Concise Guide to PHARMACOLOGY 2015/16: G protein-coupled receptors. Br.
669 J. Pharmacol. 2015;172:5744–869.

670 40. Stilling RM, van de Wouw M, Clarke G, Stanton C, Dinan TG, Cryan JF. The
671 neuropharmacology of butyrate: The bread and butter of the microbiota-gut-brain axis?
672 Neurochem. Int. 2016;99:110–32.

673 41. Schmidt J, Smith NJ, Christiansen E, Tikhonova IG, Grundmann M, Hudson BD,
674 et al. Selective orthosteric free fatty acid receptor 2 (FFA2) agonists: identification of
675 the structural and chemical requirements for selective activation of FFA2 versus FFA3.
676 J. Biol. Chem. 2011;286:10628–40.

677 42. De Vadder F, Kovatcheva-Datchary P, Goncalves D, Vinera J, Zitoun C, Duchampt
678 A, et al. Microbiota-generated metabolites promote metabolic benefits via gut-brain
679 neural circuits. Cell. 2014;156:84–96.

680 43. Burokas A, Arboleya S, Moloney RD, Peterson VL, Murphy K, Clarke G, et al.
681 Targeting the Microbiota-Gut-Brain Axis: Prebiotics Have Anxiolytic and

682 Antidepressant-like Effects and Reverse the Impact of Chronic Stress in Mice. Biol.
683 Psychiatry. 2017;82:472–87.

684 44. Byrne CS, Chambers ES, Alhabeeb H, Chhina N, Morrison DJ, Preston T, et al.
685 Increased colonic propionate reduces anticipatory reward responses in the human
686 striatum to high-energy foods. Am. J. Clin. Nutr. 2016;104:5–14.

687 45. Brown AJ, Goldsworthy SM, Barnes AA, Eilert MM, Tcheang L, Daniels D, et al.
688 The Orphan G protein-coupled receptors GPR41 and GPR43 are activated by
689 propionate and other short chain carboxylic acids. J. Biol. Chem. American Society for
690 Biochemistry and Molecular Biology; 2003;278:11312–9.

691 46. Radoshevich L, Dussurget O. Cytosolic Innate Immune Sensing and Signaling
692 upon Infection. Front. Microbiol. 2016;7:313.

693 47. Chen EY, Tan CM, Kou Y, Duan Q, Wang Z, Meirelles GV, et al. Enrichr: interactive
694 and collaborative HTML5 gene list enrichment analysis tool. BMC Bioinformatics.
695 2013;14:128.

696 48. Kuleshov M V, Jones MR, Rouillard AD, Fernandez NF, Duan Q, Wang Z, et al.
697 Enrichr: a comprehensive gene set enrichment analysis web server 2016 update.
698 Nucleic Acids Res. 2016;44:W90–7.

699 49. Helms HC, Abbott NJ, Burek M, Cecchelli R, Couraud P-O, Deli MA, et al. In vitro
700 models of the blood-brain barrier: An overview of commonly used brain endothelial
701 cell culture models and guidelines for their use. J. Cereb. Blood Flow Metab.
702 2016;36:862–90.

703 50. Haseloff RF, Dithmer S, Winkler L, Wolburg H, Blasig IE. Transmembrane proteins
704 of the tight junctions at the blood-brain barrier: structural and functional aspects.
705 Semin. Cell Dev. Biol. 2015;38:16–25.

706 51. Varatharaj A, Galea I. The blood-brain barrier in systemic inflammation. Brain.
707 Behav. Immun. 2016;60:1–12.

708 52. Peri F, Piazza M, Calabrese V, Damore G, Cighetti R. Exploring the LPS/TLR4
709 signal pathway with small molecules. Biochem. Soc. Trans. 2010;38:1390–5.

710 53. Gelain DP, Dalmolin RJS, Belau VL, Moreira JCF, Klamt F, Castro MAA. A
711 systematic review of human antioxidant genes. Front. Biosci. (Landmark Ed.
712 2009;14:4457–63.

713 54. Gorrini C, Harris IS, Mak TW. Modulation of oxidative stress as an anticancer
714 strategy. Nat. Rev. Drug Discov. 2013;12:931–47.

715 55. Todesco T, Rao A V, Bosello O, Jenkins DJ. Propionate lowers blood glucose and
716 alters lipid metabolism in healthy subjects. Am. J. Clin. Nutr. 1991;54:860–5.

717 56. Venter CS, Vorster HH, Cummings JH. Effects of dietary propionate on
718 carbohydrate and lipid metabolism in healthy volunteers. Am. J. Gastroenterol.
719 1990;85:549–53.

720 57. Reichardt N, Duncan SH, Young P, Belenguer A, McWilliam Leitch C, Scott KP, et
721 al. Phylogenetic distribution of three pathways for propionate production within the
722 human gut microbiota. ISME J. 2014;8:1323–35.

723 58. Vogt JA, Wolever TMS. Fecal acetate is inversely related to acetate absorption
724 from the human rectum and distal colon. J. Nutr. 2003;133:3145–8.

725 59. Vogt JA, Pencharz PB, Wolever TMS. L-Rhamnose increases serum propionate
726 in humans. Am. J. Clin. Nutr. 2004;80:89–94.

727 60. Nilsson AC, Östman EM, Knudsen KEB, Holst JJ, Björck IME. A Cereal-Based
728 Evening Meal Rich in Indigestible Carbohydrates Increases Plasma Butyrate the Next
729 Morning1,2. J. Nutr. 2010;140:1932–6.

730 61. Russell WR, Hoyles L, Flint HJ, Dumas M-E. Colonic bacterial metabolites and
731 human health. Curr. Opin. Microbiol. 2013;16:246–54.

732 62. Nohr MK, Egerod KL, Christiansen SH, Gille A, Offermanns S, Schwartz TW, et
733 al. Expression of the short chain fatty acid receptor GPR41/FFAR3 in autonomic and
734 somatic sensory ganglia. Neuroscience. 2015;290:126–37.

735 63. Zheng X, Xie G, Zhao A, Zhao L, Yao C, Chiu NHL, et al. The footprints of gut
736 microbial-mammalian co-metabolism. J. Proteome Res. 2011;10:5512–22.

64. Montagne A, Barnes SR, Sweeney MD, Halliday MR, Sagare AP, Zhao Z, et al. Blood-Brain Barrier Breakdown in the Aging Human Hippocampus. Neuron. 2015;85:296–302.

65. Taheri S, Gasparovic C, Huisa BN, Adair JC, Edmonds E, Prestopnik J, et al. Blood-brain barrier permeability abnormalities in vascular cognitive impairment. Stroke. 2011;42:2158–63.

66. Bowman GL, Kaye JA, Moore M, Waichunas D, Carlson NE, Quinn JF. Blood-brain barrier impairment in Alzheimer disease: stability and functional significance. Neurology. 2007;68:1809–14.

67. Wardlaw JM, Doubal FN, Valdes-Hernandez M, Wang X, Chappell FM, Shuler K, et al. Blood-brain barrier permeability and long-term clinical and imaging outcomes in cerebral small vessel disease. Stroke. 2013;44:525–7.

68. Aizawa E, Tsuji H, Asahara T, Takahashi T, Teraishi T, Yoshida S, et al. Possible association of Bifidobacterium and Lactobacillus in the gut microbiota of patients with major depressive disorder. J. Affect. Disord. 2016;202:254–7.

69. Scheperjans F, Aho V, Pereira PAB, Koskinen K, Paulin L, Pekkonen E, et al. Gut microbiota are related to Parkinson's disease and clinical phenotype. Mov. Disord. 2015;30:350–8.

70. Petrov VA, Saltykova I V, Zhukova IA, Alifirova VM, Zhukova NG, Dorofeeva YB, et al. Analysis of Gut Microbiota in Patients with Parkinson's Disease. Bull. Exp. Biol. Med. 2017;162:734–7.

71. Cattaneo A, Cattane N, Galluzzi S, Provasi S, Lopizzo N, Festari C, et al. Association of brain amyloidosis with pro-inflammatory gut bacterial taxa and peripheral inflammation markers in cognitively impaired elderly. Neurobiol. Aging. 2017;49:60–8.

72. Bedarf JR, Hildebrand F, Coelho LP, Sunagawa S, Bahram M, Goeser F, et al. Functional implications of microbial and viral gut metagenome changes in early stage L-DOPA-naive Parkinson's disease patients. Genome Med. 2017;9:39.

765 73. Akbari E, Asemi Z, Daneshvar Kakhaki R, Bahmani F, Kouchaki E, Tamtaji OR, et
766 al. Effect of Probiotic Supplementation on Cognitive Function and Metabolic Status in
767 Alzheimer's Disease: A Randomized, Double-Blind and Controlled Trial. Front. Aging
768 Neurosci. 2016;8:256.

769 74. Kouchaki E, Tamtaji OR, Salami M, Bahmani F, Daneshvar Kakhaki R, Akbari E,
770 et al. Clinical and metabolic response to probiotic supplementation in patients with
771 multiple sclerosis: A randomized, double-blind, placebo-controlled trial. Clin. Nutr.
772 2016;36:1245–9.

773 75. Engelhardt B, Sorokin L. The blood-brain and the blood-cerebrospinal fluid
774 barriers: function and dysfunction. Semin. Immunopathol. 2009;31:497–511.

775 76. Gonçalves P, Araújo JR, Pinho MJ, Martel F. Modulation of butyrate transport in
776 Caco-2 cells. Naunyn. Schmiedebergs. Arch. Pharmacol. 2009;379:325–36.

777 77. Stein J, Zores M, Schröder O. Short-chain fatty acid (SCFA) uptake into Caco-2
778 cells by a pH-dependent and carrier mediated transport mechanism. Eur. J. Nutr.
779 2000;39:121–5.

780 78. Pariante CM. Why are depressed patients inflamed? A reflection on 20 years of
781 research on depression, glucocorticoid resistance and inflammation. Eur.
782 Neuropsychopharmacol. 2017;27:554–9.

783 79. Cristante E, McArthur S, Mauro C, Maggioli E, Romero IAIA, Wylezinska-Arridge
784 M, et al. Identification of an essential endogenous regulator of blood-brain barrier
785 integrity, and its pathological and therapeutic implications. Proc. Natl. Acad. Sci. U. S.
786 A. 2013/01/02 ed. 2013;110:832–41.

787 80. Weksler BB, Subileau EA, Perrière N, Charneau P, Holloway K, Leveque M, et al.
788 Blood-brain barrier-specific properties of a human adult brain endothelial cell line.
789 FASEB J. 2005;19:1872–4.

790 81. Maggioli E, McArthur S, Mauro C, Kieswich J, Kusters DHMHM, Reutelingsperger
791 CPMPM, et al. Estrogen protects the blood-brain barrier from inflammation-induced
792 disruption and increased lymphocyte trafficking. BRAIN, Behav. Immun. 2015;51:212–
793 22.

794 82. Gautier L, Cope L, Bolstad BM, Irizarry RA. affy--analysis of Affymetrix GeneChip
795 data at the probe level. Bioinformatics. 2004;20:307–15.

796 83. Dunning M, Lynch A, Eldridge M. illuminaHumanv4.db: Illumina HumanHT12v4
797 annotation data (chip illuminaHumanv4). 2015.

798 84. Ritchie ME, Dunning MJ, Smith ML, Shi W, Lynch AG. BeadArray expression
799 analysis using bioconductor. Lewitter F, editor. PLoS Comput. Biol. 2011;7:e1002276.

800 85. Tarca AL, Draghici S, Khatri P, Hassan SS, Mittal P, Kim J-S, et al. A novel
801 signaling pathway impact analysis. Bioinformatics. 2009;25:75–82.

802 86. Abbott NJ, Hughes CC, Revest PA, Greenwood J. Development and
803 characterisation of a rat brain capillary endothelial culture: towards an in vitro blood-
804 brain barrier. J. Cell Sci. 1992;103 (Pt 1:23–37.

805 87. Coisne C, Dehouck L, Faveeuw C, Delplace Y, Miller F, Landry C, et al. Mouse
806 syngenic in vitro blood-brain barrier model: a new tool to examine inflammatory events
807 in cerebral endothelium. Lab. Invest. 2005;85:734–46.

808 88. Pais de Barros J-P, Gautier T, Sali W, Adrie C, Choubley H, Charron E, et al.
809 Quantitative lipopolysaccharide analysis using HPLC/MS/MS and its combination with
810 the limulus amebocyte lysate assay. J. Lipid Res. American Society for Biochemistry
811 and Molecular Biology; 2015;56:1363–9.

812 89. Löscher W, Potschka H. Blood-brain barrier active efflux transporters: ATP-binding
813 cassette gene family. NeuroRx. Am. Soc. for Experimental NeuroTherapeutics;
814 2005;2:86–98.

815 90. Wishart DS, Jewison T, Guo AC, Wilson M, Knox C, Liu Y, et al. HMDB 3.0--The
816 Human Metabolome Database in 2013. Nucleic Acids Res. 2013;41:D801–7.

817 91. Ritchie ME, Phipson B, Wu D, Hu Y, Law CW, Shi W, et al. limma powers
818 differential expression analyses for RNA-sequencing and microarray studies. Nucleic
819 Acids Res. 2015;43:e47.

820

Figure Legends

Fig. 1: Effects on gene expression of exposure of the hCMEC/D3 cell line to propionate (1 μM, 24 h). (a) Representative images of FFAR3 immunoreactivity within endothelial cells of capillaries (i) and larger post-capillary (ii) blood vessels in control human brains *post mortem*; scale bar 20 μm, sections are 5 μm thick; images are representative of five independent cases, areas of particular immunoreactivity are highlighted by black arrowheads. (b) Surface expression of FFAR3/GPR41 by hCMEC/D3 cells (grey line, unstained cells, black line secondary antibody control, red line FFAR3), data are representative of three independent experiments. (c) Volcano plot showing significantly ($P_{FDR} < 0.1$, red dots) differentially expressed genes. The top 20 up- and down-regulated genes are labelled. (d) SPIA evidence plot for the 1136 significantly differentially expressed genes. Only those human KEGG pathways associated with non-specific microbial infections are labelled. The pathways at the right of the red oblique line are significant ($P < 0.2$) after Bonferroni correction of the global *P* values, pG, obtained by combining the pPERT and pNDE using the normal inversion method. The pathways at the right of the blue oblique line are significant ($P < 0.2$) after a FDR correction of the global *P* values, pG. 04810, Regulation of actin cytoskeleton (inhibited); 04064, NF-kappa B signaling pathway (inhibited); 04978, Mineral absorption (inhibited); 03013, RNA transport (activated); 04141, Protein processing in endoplasmic reticulum (activated); 04350, TGF-beta signaling pathway (activated); 04623, Cytosolic DNA-sensing pathway (inhibited). (e) Association of all significantly differentially expressed genes ($n = 1136$) with KEGG pathways, Enrichr. (f) Association of all significantly upregulated genes ($n = 553$) with WikiPathways, Enrichr. (e, f) The lighter in colour and the longer the bars, the more significant the

result is. Significance of data was determined using rank-based ranking; only the top 10 results are shown in each case.

Fig. 2: Protective effects of propionate against LPS-induced barrier disruption. (a) Assessment of the paracellular permeability of hCMEC/D3 monolayers to 70 kDa FITC-dextran following treatment for 24 h with 65 µM acetate, 1 µM butyrate or 1 µM propionate, with or without inclusion of 50 ng/ml LPS for the last 12 h of incubation; data are mean ± SEM, *n* = 3 independent experiments. (b) Trans-endothelial electrical resistance of hCMEC/D3 monolayers following treatment for 24 h with 65 µM acetate, 1 µM butyrate or 1 µM propionate, with or without inclusion of 50 ng/ml LPS for the last 12 h of incubation; data are mean ± SEM, *n* = 3 independent experiments. (c) Confocal microscopic analysis of expression of the tight junction components claudin-5, occludin and zona occludens-1 (ZO-1) in hCMEC/D3 cells following treatment for 24 h with 1 µM propionate, with or without inclusion of 50 ng/ml LPS for the last 12 h of incubation. Scale bar (10 µm) applies to all images. Images are representative of at least three independent experiments. (d) Expression of *CD14* mRNA in control and propionate-treated (1 µM; 24 h) hCMEC/D3 cells according to microarray data (data are mean ± SEM, *n* = 3). (e) Surface expression of CD14 protein on control and propionate-treated hCMEC/D3 cells (grey line, unstained cells, black line secondary antibody control, red line FFAR3), data are representative of three independent experiments. (f) Median fluorescence intensity of surface expression of CD14 protein on control and propionate-treated hCMEC/D3 cells, dashed line indicates isotype control fluorescence intensity; data are mean ± SEM, *n*=3 independent experiments.

Fig. 3: Protective effects of propionate against oxidative stress. (a) Representation of stress-response genes significantly upregulated in the current study and directly influenced by NFE2L2, '*the master regulator of antioxidant responses*' [54]. (b) Confocal microscopic analysis of expression of NFE2L2 (Nrf2) in hCMEC/D3 cells following treatment for 24 h with 1 μM propionate; scale bar (10 μm) applies to all images. Images are representative of at least three independent experiments. (c) Production of reactive oxygen species (ROS) in control and propionate pre-treated (1 μM, 24 h) hCMEC/D3 cells treated for 30 min with the mitochondrial complex I inhibitor rotenone (2.5 μM). Data are mean ± SEM, *n*=3 independent experiments.

Fig. 4: Production of propionate by the human gut microbiota. Propionate can be produced directly or indirectly by cross-feeding from succinate- and lactate-producers (e.g. *Selenomonas*, *Megasphaera* and *Veillonella* spp.). Image produced using information taken from [57]. **Akkermansia muciniphila* is known to produce propionate; it is thought to do this via the succinate pathway [57].

Supplementary Fig. 1: Persistence of the protective effect of propionate upon LPS-induced barrier disruption across different doses. (a) Assessment of the paracellular permeability of hCMEC/D3 monolayers to 70 kDa FITC-dextran following treatment for 24 h with 1, 10 or 100 μM propionate, with or without inclusion of 50 ng/ml LPS for the last 12 h of incubation; data are mean ± SEM, *n* = 3 independent experiments. (b) Trans-endothelial electrical resistance of hCMEC/D3 monolayers following treatment for 24 h with 1, 10 or 100 μM propionate, with or without inclusion of 50 ng/ml LPS for the last 12 h of incubation; data are mean ± SEM, *n* = 3 independent experiments.

Supplementary Fig. 2: Protective effects of propionate against LPS-induced barrier disruption in primary human brain microvascular endothelial cells (HBMEC). (a) Assessment of the paracellular permeability of HBMEC monolayers to 70 kDa FITC-dextran following treatment for 24 h with 1 µM propionate, with or without inclusion of 50 ng/ml LPS for the last 12 h of incubation; data are mean ± SEM, *n* = 3 independent experiments. (b) Trans-endothelial electrical resistance of HBMEC monolayers following treatment for 24 h with 1 µM propionate, with or without inclusion of 50 ng/ml LPS for the last 12 h of incubation; data are mean ± SEM, *n* = 3 independent experiments.

Supplementary Fig. 3: Effects of propionate upon expression and activity of typical cerebromicrovascular efflux transporter systems. (a) Surface expression of BCRP, LRP-1 and P-glycoprotein on control and propionate-treated (1 µM, 24 h) hCMEC/D3 cells (black, control, red, propionate), data are representative of three independent experiments. (b) Median fluorescence intensity of surface expression of BCRP, LRP-1 and P-glycoprotein on control and propionate-treated (1 µM, 24 h) hCMEC/D3 cells; data are mean ± SEM, *n*=3 independent experiments. (c) Lack of stimulatory effect of propionate upon BCRP, data are mean ± SEM, *n* = 4. (d) Lack of inhibitory effect of propionate upon stimulated ATP-dependent activity of BCRP, data are mean ± SEM, *n* = 4. (e) Lack of stimulatory effect of propionate upon P-glycoprotein, data are mean ± SEM, *n* = 4. (f) Lack of inhibitory effect of propionate upon stimulated ATP-dependent activity of P-glycoprotein, data are mean ± SEM, *n* = 4.

Supplementary Table 1: Effects of propionate treatment (1 µM, 24 h) upon mRNA expression of BBB-related genes in hCMEC/D3 cells, grouped in broad functional categories. Gene names listed in bold were significantly regulated compared to untreated cells ($P_{FDR} < 0.05$)

Supplementary Table 2: Effects of propionate treatment (1 µM, 24 h) upon mRNA expression of antioxidant system-related genes in hCMEC/D3 cells. Gene names listed in bold were significantly regulated compared to untreated cells ($P_{FDR} < 0.05$).

Figure 1

a)

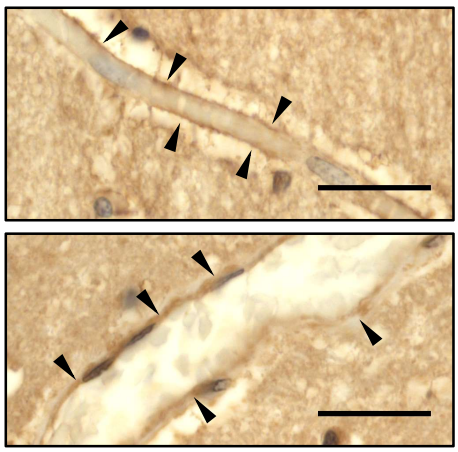

b)

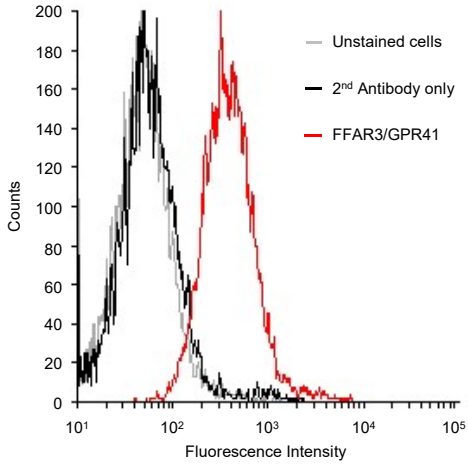

c)

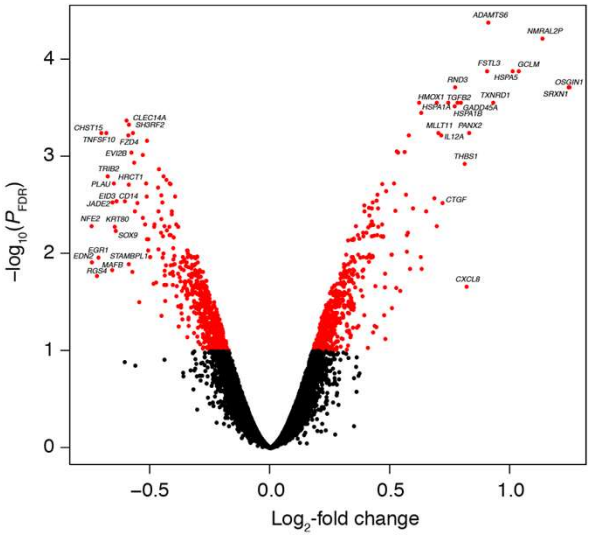

d)

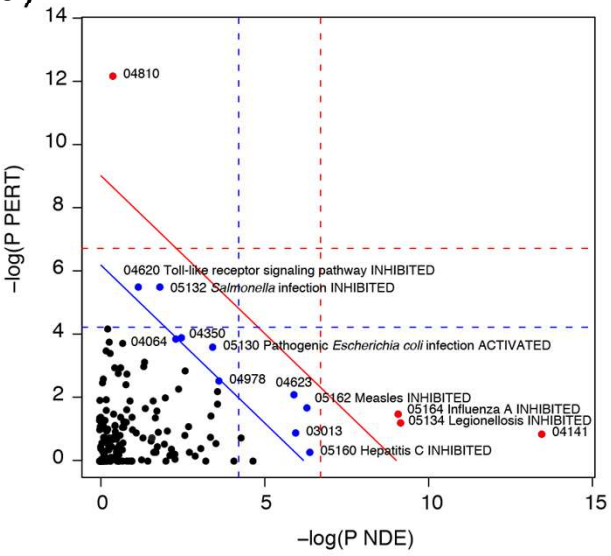

e)

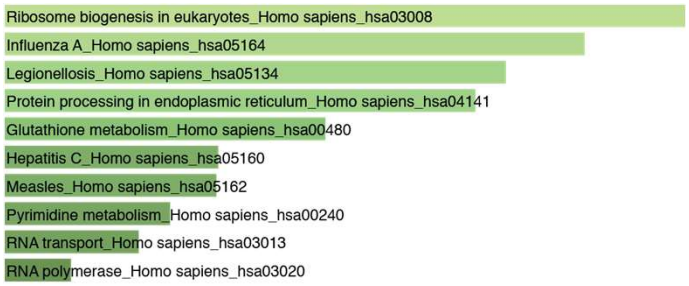

f)

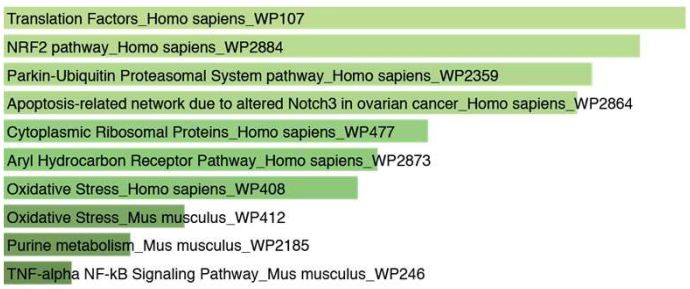

Figure 2

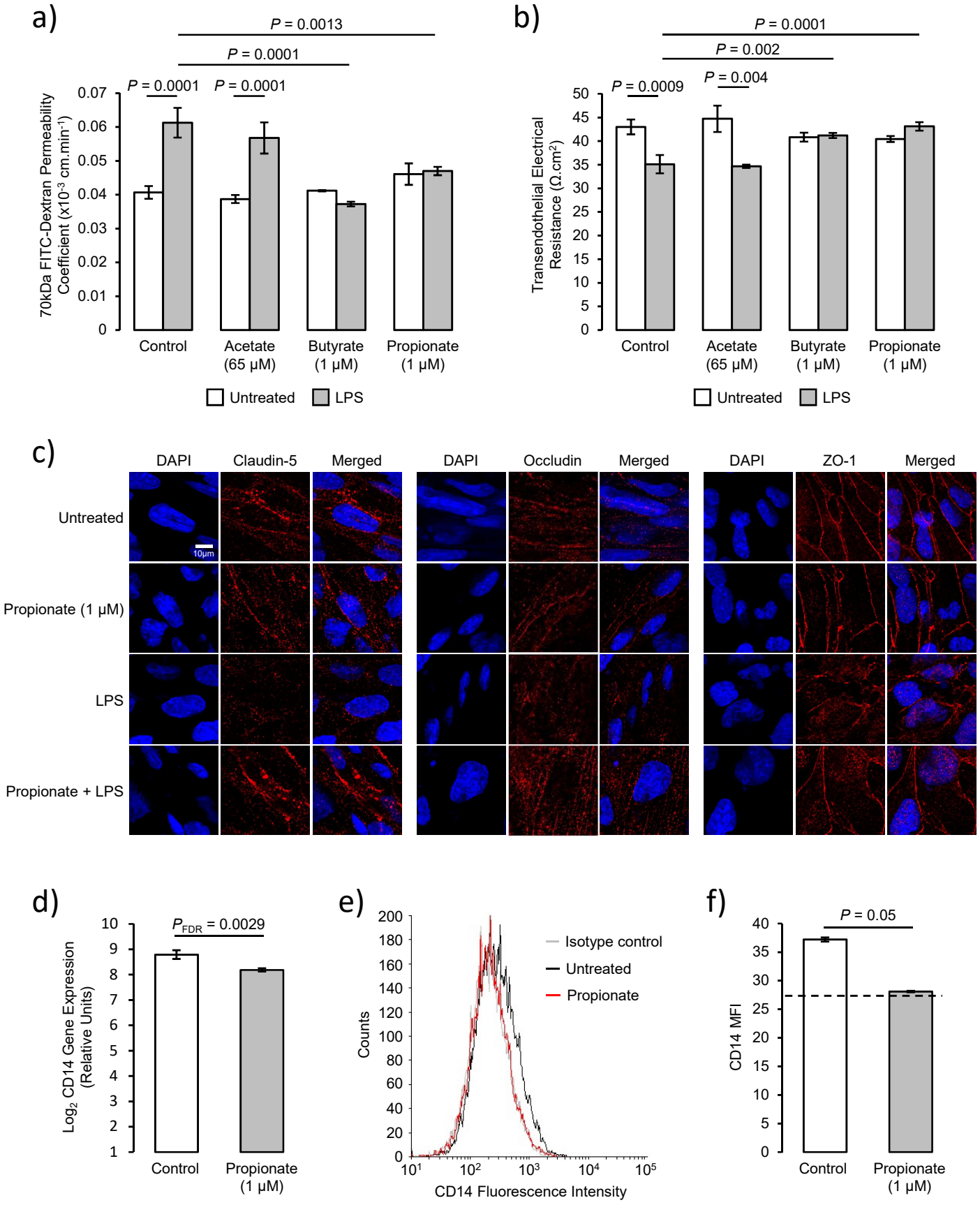
a)
P = 0.0013
P = 0.0001
P = 0.0001
P = 0.0001
70kDa FITC-Dextran Permeability Coefficient (x10-3 cm.min-1)
0.07
0.06
0.05
0.04
0.03
0.02
0.01
0
Control
Acetate (65 µM)
Butyrate (1 µM)
Propionate (1 µM)
Untreated
LPS
b)
P = 0.0001
P = 0.002
P = 0.004
P = 0.0009
Transendothelial Electrical Resistance (Ω.cm2)
50
45
40
35
30
25
20
15
10
5
0
Control
Acetate (65 µM)
Butyrate (1 µM)
Propionate (1 µM)
Untreated
LPS
c)
DAPI
Claudin-5
Merged
DAPI
Occludin
Merged
DAPI
ZO-1
Merged
Untreated
Propionate (1 µM)
LPS
Propionate + LPS
10µm
d)
PFDR = 0.0029
Log2 CD14 Gene Expression (Relative Units)
10
9
8
7
6
5
4
3
2
1
Control
Propionate (1 µM)
e)
Isotype control
Untreated
Propionate
Counts
200
180
160
140
120
100
80
60
40
20
0
10¹
10²
10³
10⁴
10⁵
CD14 Fluorescence Intensity
f)
P = 0.05
CD14 MFI
40
35
30
25
20
15
10
5
0
Control
Propionate (1 µM)

Figure 3

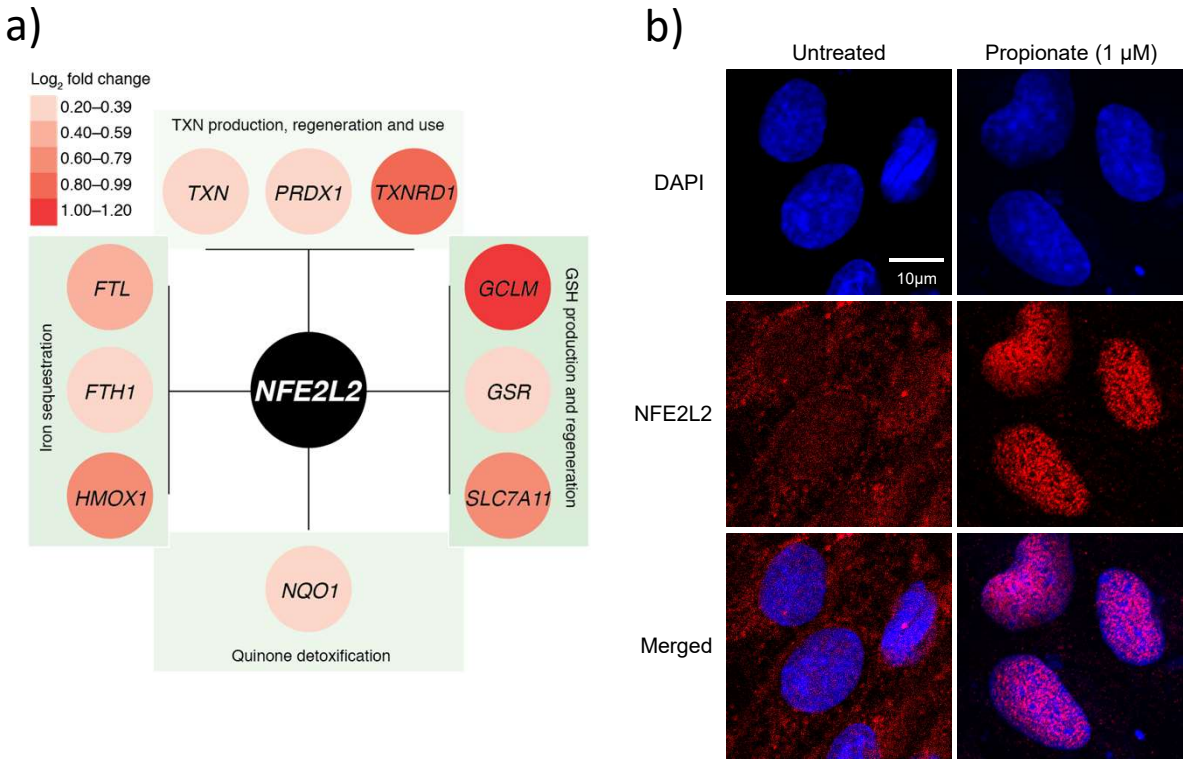
a)
Log2 fold change
0.20–0.39
0.40–0.59
0.60–0.79
0.80–0.99
1.00–1.20
TXN production, regeneration and use
TXN
PRDX1
TXNRD1
FTL
FTH1
HMOX1
Iron sequestration
NFE2L2
GCLM
GSR
SLC7A11
GSH production and regeneration
NQO1
Quinone detoxification
b)
Untreated
Propionate (1 μM)
DAPI
NFE2L2
Merged
10μm

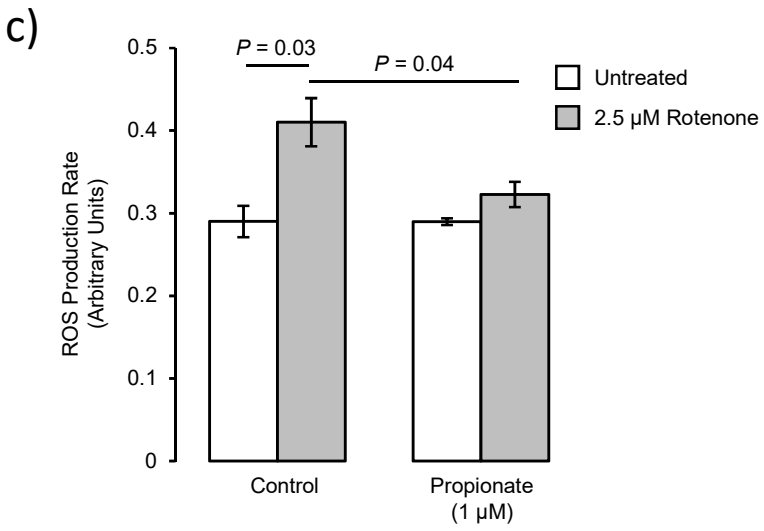
c)
P = 0.03
P = 0.04
Untreated
2.5 μM Rotenone
ROS Production Rate
(Arbitrary Units)
0.5
0.4
0.3
0.2
0.1
0
Control
Propionate
(1 μM)

Figure 4

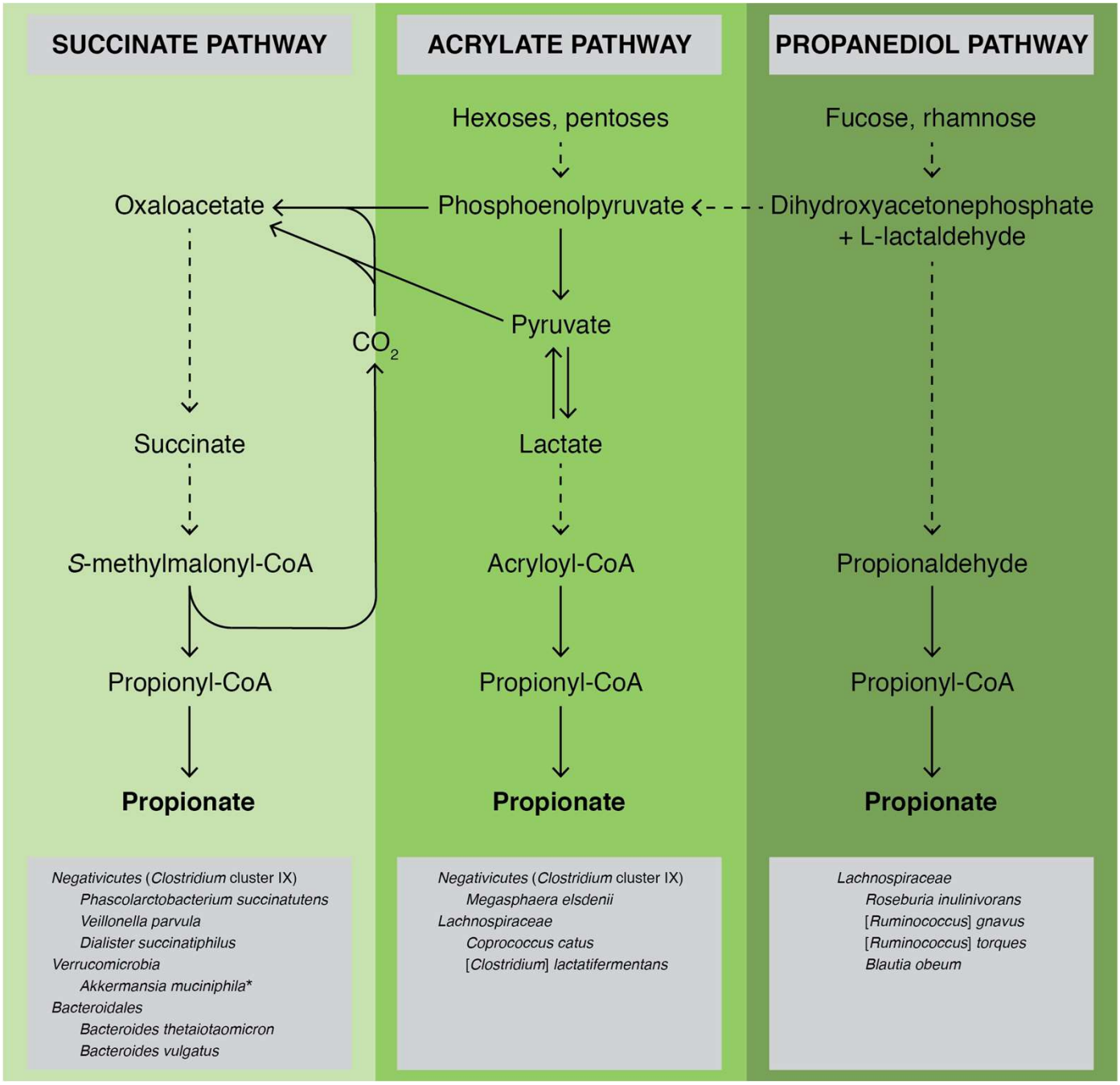
SUCCINATE PATHWAY
ACRYLATE PATHWAY
PROPANEDIOL PATHWAY
Hexoses, pentoses
Fucose, rhamnose
Oxaloacetate
Phosphoenolpyruvate
Dihydroxyacetonephosphate + L-lactaldehyde
Pyruvate
CO_2
Succinate
Lactate
S-methylmalonyl-CoA
Acryloyl-CoA
Propionaldehyde
Propionyl-CoA
Propionyl-CoA
Propionyl-CoA
Propionate
Propionate
Propionate
Negativicutes (Clostridium cluster IX)
Phascolarctobacterium succinatutens
Veillonella parvula
Dialister succinatiphilus
Verrucomicrobia
Akkermansia muciniphila*
Bacteroidales
Bacteroides thetaiotaomicron
Bacteroides vulgatus
Negativicutes (Clostridium cluster IX)
Megasphaera elsdenii
Lachnospiraceae
Coprococcus catus
[Clostridium] lactatifermentans
Lachnospiraceae
Roseburia inulinivorans
[Ruminococcus] gnavus
[Ruminococcus] torques
Blautia obeum

Supplementary Figure 1

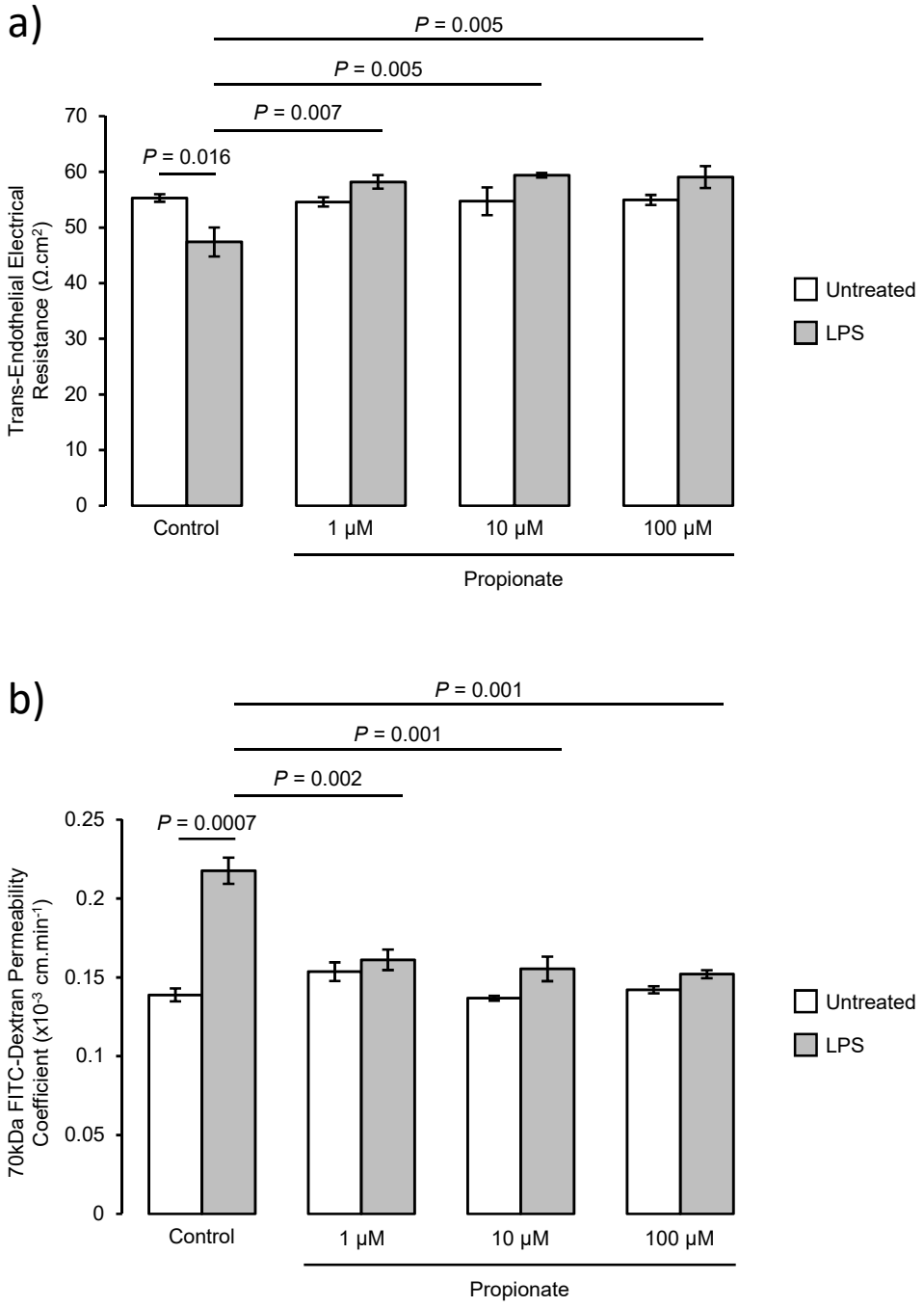

Supplementary Figure 2

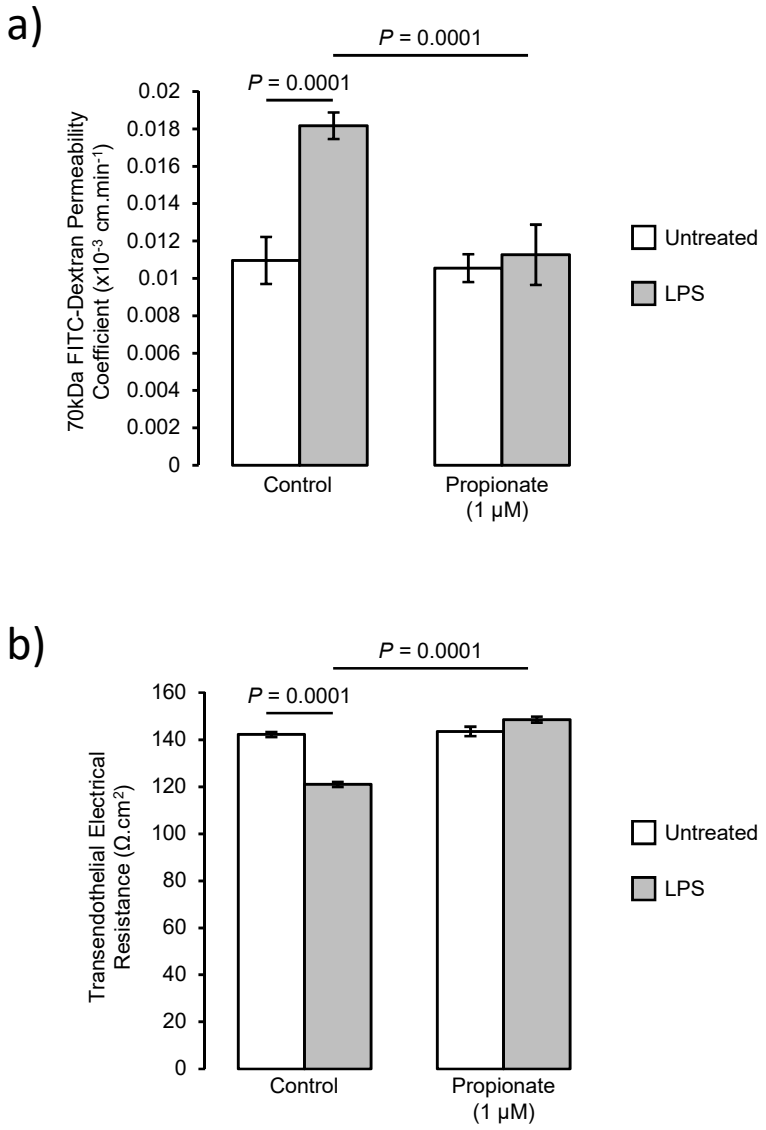

Supplementary Figure 3

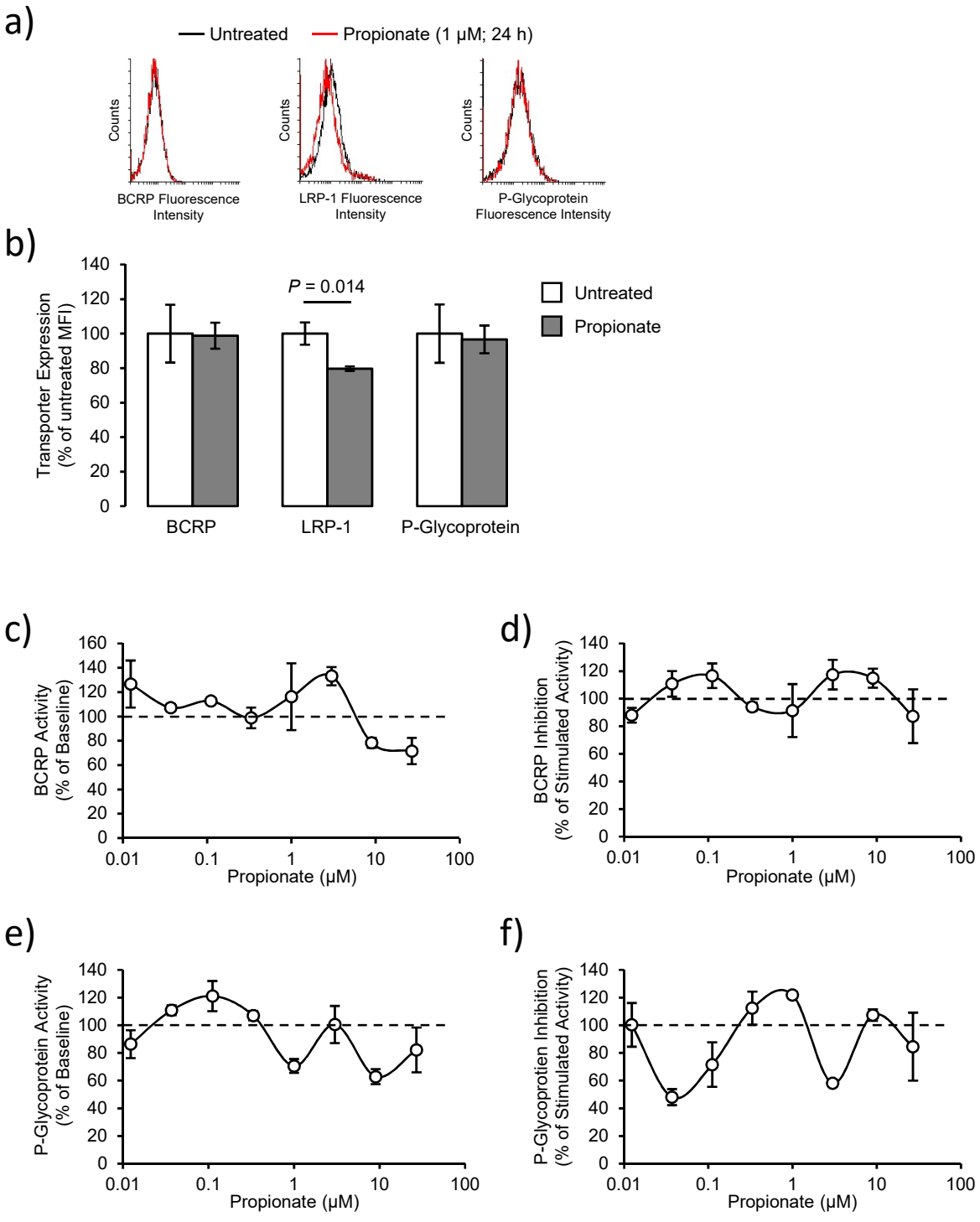

Cell Adhesion/Junctional proteins/Cytoskeletal factors

Symbol	Description	logFC	adj.P.Val
PECAM1	**platelet and endothelial cell adhesion molecule 1**	**-0.518**	**0.002**
CLDN11	**claudin 11**	**0.541**	**0.024**
GJA1	gap junction protein alpha 1	0.434	0.055
CLDN1	claudin 1	0.264	0.062
JAM3	junctional adhesion molecule 3	0.180	0.132
UTRN	utrophin	-0.155	0.157
CDH2	cadherin 2	0.167	0.184
CLDN7	claudin 7	-0.122	0.270
ANXA1	annexin A1	0.145	0.270
TJP2	tight junction protein 2	-0.124	0.281
CLDN17	claudin 17	-0.124	0.282
CLDN4	claudin 4	0.141	0.341
SMARCA2	SWI/SNF related, matrix associated, actin dependent regulator of chromatin, subfamily a, member 2	0.118	0.373
CLDN23	claudin 23	-0.108	0.462
JAM2	junctional adhesion molecule 2	-0.110	0.540
TJP1	tight junction protein 1	0.090	0.573
CLDN6	claudin 6	0.092	0.582
LAMA4	laminin subunit alpha 4	-0.078	0.629
LAMA3	laminin subunit alpha 3	-0.070	0.657
DAG1	dystroglycan 1	-0.067	0.663
CLDN20	claudin 20	0.073	0.666
AGRN	agrin	0.055	0.694
CLDN12	claudin 12	0.064	0.751
CLDN8	claudin 8	-0.049	0.753
CLDN15	claudin 15	-0.050	0.778
CTNNB1	catenin beta 1	-0.047	0.783
VIM	vimentin	0.041	0.792
HAPLN2	hyaluronan and proteoglycan link protein 2	-0.054	0.794
DTNA	dystrobrevin alpha	0.053	0.796
ESAM	endothelial cell adhesion molecule	-0.043	0.799
LAMB2	laminin subunit beta 2	-0.044	0.803
CLDN9	claudin 9	-0.039	0.804
LAMA2	laminin subunit alpha 2	-0.057	0.808
ITM2A	integral membrane protein 2A	-0.041	0.837
FN1	fibronectin 1	-0.037	0.852
COL4A1	collagen type IV alpha 1 chain	0.030	0.875
TJP3	tight junction protein 3	-0.027	0.894
CLDN3	claudin 3	-0.023	0.906
GJB6	gap junction protein beta 6	0.022	0.911
CDH5	cadherin 5	-0.029	0.920
LAMA1	laminin subunit alpha 1	0.014	0.948
CLDN5	claudin 5	-0.016	0.962
CLDN22	claudin 22	0.013	0.963
ACTB	actin beta	0.009	0.965
CLDN10	claudin 10	-0.009	0.966
ADGRA2	adhesion G protein-coupled receptor A2	0.010	0.966
ITGA3	integrin subunit alpha 3	-0.009	0.967

OCLN	occludin	-0.007	0.969
HSPG2	heparan sulfate proteoglycan 2	0.008	0.973
DMD	dystrophin	-0.003	0.989
AFDN	afadin, adherens junction formation factor	0.003	0.989
MARVELD2	MARVEL domain containing 2	-0.001	0.996

Transporter proteins

Symbol	Description	logFC	adj.P.Val
SLC1A5	**solute carrier family 1 member 5**	**0.400**	**0.011**
SLC44A1	**solute carrier family 44 member 1**	**-0.261**	**0.030**
SLC7A5	solute carrier family 7 member 5	0.206	0.092
TFRC	transferrin receptor	0.262	0.099
SLC38A5	solute carrier family 38 member 5	0.194	0.165
SLC38A3	solute carrier family 38 member 3	0.140	0.240
SLC22A5	solute carrier family 22 member 5	0.140	0.272
SLC29A4	solute carrier family 29 member 4	0.144	0.299
SLC22A8	solute carrier family 22 member 8	-0.126	0.308
SLC2A1	solute carrier family 2 member 1	-0.129	0.342
SLC38A2	solute carrier family 38 member 2	0.120	0.381
SLC28A2	solute carrier family 28 member 2	0.133	0.411
SLC5A1	solute carrier family 5 member 1	0.100	0.447
SLC5A6	solute carrier family 5 member 6	0.094	0.452
SLC6A6	solute carrier family 6 member 6	0.096	0.461
SLC1A4	solute carrier family 1 member 4	-0.115	0.462
SLC27A4	solute carrier family 27 member 4	-0.139	0.463
LRP2	LDL receptor related protein 2	0.082	0.501
SLC38A1	solute carrier family 38 member 1	0.091	0.510
SLC22A1	solute carrier family 22 member 1	0.078	0.560
LDLR	low density lipoprotein receptor	-0.075	0.566
SLC1A3	solute carrier family 1 member 3	0.084	0.581
MFSD2A	major facilitator superfamily domain containing 2A	0.079	0.593
ABCG2	ATP binding cassette subfamily G member 2 (Junior blood group)	0.066	0.671
INSR	insulin receptor	0.060	0.718
AQP4	aquaporin 4	0.060	0.733
SLC16A2	solute carrier family 16 member 2	-0.057	0.780
ABCC5	ATP binding cassette subfamily C member 5	-0.041	0.793
SLCO1C1	solute carrier organic anion transporter family member 1C1	0.041	0.795
SLC29A1	solute carrier family 29 member 1 (Augustine blood group)	0.036	0.807
SLC27A1	solute carrier family 27 member 1	-0.036	0.818
SLC7A3	solute carrier family 7 member 3	0.038	0.824
SLC22A2	solute carrier family 22 member 2	0.035	0.843
SLC16A1	solute carrier family 16 member 1	-0.047	0.847
ABCB1	ATP binding cassette subfamily B member 1	0.029	0.866
AGER	advanced glycosylation end-product specific receptor	-0.026	0.908
AVPR1A	arginine vasopressin receptor 1A	-0.023	0.912
ABCA2	ATP binding cassette subfamily A member 2	0.015	0.947
SLC6A9	solute carrier family 6 member 9	0.013	0.949
SLC1A1	solute carrier family 1 member 1	-0.013	0.954
SLC7A1	solute carrier family 7 member 1	0.013	0.955
ABCC1	ATP binding cassette subfamily C member 1	0.012	0.956

SLC22A3	solute carrier family 22 member 3	-0.012	0.957
LEPR	leptin receptor	-0.009	0.960
SLC16A7	solute carrier family 16 member 7	-0.012	0.962
ABCC4	ATP binding cassette subfamily C member 4	-0.011	0.963
SLC5A3	solute carrier family 5 member 3	-0.009	0.967
SLC7A6	solute carrier family 7 member 6	-0.008	0.969
SLCO2B1	solute carrier organic anion transporter family member 2B1	-0.005	0.983
ABCC2	ATP binding cassette subfamily C member 2	-0.003	0.988
SLCO1B1	solute carrier organic anion transporter family member 1B1	0.003	0.988
SLC2A13	solute carrier family 2 member 13	0.003	0.990
SLC1A2	solute carrier family 1 member 2	0.001	0.995

Inflammatory response

Symbol	Description	logFC	adj.P.Val
TNFSF10	**tumor necrosis factor superfamily member 10**	**-0.684**	**0.001**
PDGFRB	**platelet derived growth factor receptor beta**	**-0.441**	**0.015**
TNFRSF1A	**TNF receptor superfamily member 1A**	**-0.289**	**0.021**
TNFRSF12A	**TNF receptor superfamily member 12A**	**0.383**	**0.028**
TNFRSF21	**TNF receptor superfamily member 21**	**0.325**	**0.031**
ITGB4	integrin subunit beta 4	-0.205	0.056
TNFAIP6	TNF alpha induced protein 6	0.325	0.118
PODXL	podocalyxin like	-0.194	0.130
ITGA5	integrin subunit alpha 5	-0.211	0.163
ITGA1	integrin subunit alpha 1	-0.150	0.188
PTGS2	prostaglandin-endoperoxide synthase 2	0.187	0.189
ITGB5	integrin subunit beta 5	-0.156	0.193
CXCL2	C-X-C motif chemokine ligand 2	0.171	0.231
IKBKB	inhibitor of nuclear factor kappa B kinase subunit beta	-0.139	0.299
SOD1	superoxide dismutase 1, soluble	0.126	0.338
ITGB8	integrin subunit beta 8	-0.144	0.340
NOS1	nitric oxide synthase 1	0.114	0.366
CCR5	C-C motif chemokine receptor 5 (gene/pseudogene)	0.222	0.391
ITGA4	integrin subunit alpha 4	0.161	0.430
CLEC5A	C-type lectin domain family 5 member A	0.138	0.441
ITGA6	integrin subunit alpha 6	-0.092	0.442
GRN	granulin precursor	-0.089	0.455
MMP9	matrix metallopeptidase 9	-0.099	0.475
NR3C1	nuclear receptor subfamily 3 group C member 1	-0.085	0.496
CRH	corticotropin releasing hormone	-0.092	0.558
AGT	angiotensinogen	-0.091	0.594
PTGDS	prostaglandin D2 synthase	-0.097	0.596
NOX4	NADPH oxidase 4	0.070	0.601
MMP2	matrix metallopeptidase 2	-0.088	0.687
SELP	selectin P	-0.074	0.689
IL1RN	interleukin 1 receptor antagonist	0.060	0.692
CXCR3	C-X-C motif chemokine receptor 3	-0.060	0.711
F11R	F11 receptor	-0.089	0.741
TNFRSF1B	TNF receptor superfamily member 1B	-0.098	0.760
SEMA7A	semaphorin 7A (John Milton Hagen blood group)	0.054	0.770
ITGB3	integrin subunit beta 3	0.049	0.793

ITGAV	integrin subunit alpha V	-0.033	0.837
TLR2	toll like receptor 2	0.030	0.860
ITGB1	integrin subunit beta 1	0.026	0.880
PTGER3	prostaglandin E receptor 3	-0.022	0.895
TNF	tumor necrosis factor	-0.016	0.927
ITGB2	integrin subunit beta 2	-0.012	0.951
IL1B	interleukin 1 beta	-0.033	0.967
CCR2	C-C motif chemokine receptor 2	-0.007	0.970
CD276	CD276 molecule	0.006	0.973
C3	complement C3	-0.001	0.997

Vascular function/coagulation cascade

Symbol	Description	logFC	adj.P.Val
SERPINE2	**serpin family E member 2**	**0.461**	**0.007**
PROCR	**protein C receptor**	**0.240**	**0.046**
PLAT	plasminogen activator, tissue type	-0.242	0.051
SERPINE1	serpin family E member 1	0.244	0.212
PROS1	protein S (alpha)	-0.165	0.262
PROC	protein C, inactivator of coagulation factors Va and VIIIa	-0.128	0.479
CA1	carbonic anhydrase 1	0.081	0.518
VWF	von Willebrand factor	-0.139	0.567
AVP	arginine vasopressin	-0.057	0.758
SERPINI1	serpin family I member 1	-0.033	0.840
PLG	plasminogen	-0.030	0.884
KNG1	kininogen 1	-0.024	0.898
NOS3	nitric oxide synthase 3	0.037	0.905
MYLK	myosin light chain kinase	-0.014	0.949
PTAFR	platelet activating factor receptor	-0.013	0.952
EPAS1	endothelial PAS domain protein 1	0.010	0.955

Endothelial proliferation/angiogenesis

Symbol	Description	logFC	adj.P.Val
PDGFB	platelet derived growth factor subunit B	-0.226	0.090
TMEFF2	transmembrane protein with EGF like and two follistatin like domains 2	0.166	0.170
S100A12	S100 calcium binding protein A12	0.143	0.245
FGF19	fibroblast growth factor 19	-0.157	0.354
IGFBP3	insulin like growth factor binding protein 3	0.091	0.486
RGS5	regulator of G-protein signaling 5	-0.075	0.548
FLT1	fms related tyrosine kinase 1	-0.112	0.572
HNRNPDL	heterogeneous nuclear ribonucleoprotein D like	-0.084	0.601
VEGFA	vascular endothelial growth factor A	-0.072	0.617
S100B	S100 calcium binding protein B	-0.071	0.643
EZH1	enhancer of zeste 1 polycomb repressive complex 2 subunit	-0.068	0.722
PTPRB	protein tyrosine phosphatase, receptor type B	-0.057	0.745
HMGB1	high mobility group box 1	0.044	0.775
PTN	pleiotrophin	-0.029	0.920
KDR	kinase insert domain receptor	0.022	0.934
BTG2	BTG anti-proliferation factor 2	0.012	0.958
EPO	erythropoietin	-0.011	0.963

Other BBB-related genes

Symbol	Description	logFC	adj.P.Val
EPHA2	EPH receptor A2	-0.249	0.076
MOG	myelin oligodendrocyte glycoprotein	-0.090	0.546
CLN3	CLN3, battenin	-0.085	0.566
SRGN	serglycin	0.072	0.574
MBP	myelin basic protein	-0.066	0.646
RAMP2	receptor activity modifying protein 2	0.054	0.713
CLCN2	chloride voltage-gated channel 2	-0.055	0.733
CPE	carboxypeptidase E	0.044	0.811
CYBB	cytochrome b-245 beta chain	0.033	0.856
MPZL1	myelin protein zero like 1	0.028	0.864
GAB2	GRB2 associated binding protein 2	-0.030	0.866
MAP3K7	mitogen-activated protein kinase kinase kinase 7	0.028	0.882
APP	amyloid beta precursor protein	-0.044	0.890
APLP2	amyloid beta precursor like protein 2	0.022	0.914
PLP1	proteolipid protein 1	0.019	0.935
HDC	histidine decarboxylase	0.007	0.985
HRH3	histamine receptor H3	0.003	0.989
APOE	apolipoprotein E	0.000	1.000
GFAP	glial fibrillary acidic protein	0.000	1.000

Supplementary Table 2: Human anti-oxidant genes included in array analyses in this study

Symbol	log_2 fold change	Adjusted *P* value	Synonyms	Description
GCLM†	**1.034**	**1.312×10^{-4}**	**GLCLR**	**glutamate-cysteine ligase modifier subunit**
SRXN1	**1.242**	**1.934×10^{-4}**	**C20orf139, Npn3, SRX, SRX1**	**sulfiredoxin 1**
TXNRD1*	**0.928**	**2.770×10^{-4}**	**GRIM-12, TR, TR1, TRXR1, TXNR**	**thioredoxin reductase 1**
HMOX1†	**0.693**	**2.770×10^{-4}**	**HMOX1D, HO-1, HSP32, bK286B10**	**heme oxygenase 1**
FTL†	**0.564**	**2.467×10^{-3}**	**LFTD, NBIA3**	**ferritin light chain**
SLC7A11†	**0.649**	**3.676×10^{-3}**	**CCBR1, xCT**	**solute carrier family 7 member 11**
TXNL4B	**0.388**	**6.601×10^{-3}**	**DLP, Dim2**	**thioredoxin like 4B**
NQO1†	**0.345**	**0.015**	**DHQU, DIA4, DTD, NMOR1, NMORI, QR1**	**NAD(P)H quinone dehydrogenase 1**
TXNDC9	**0.346**	**0.020**	**APACD, PHLP3**	**thioredoxin domain containing 9**
PRDX1*	**0.306**	**0.021**	**MSP23, NKEF-A, NKEFA, PAG, PAGA, PAGB, PRX1, PRXI, TDPX2**	**peroxiredoxin 1**
MT1F	**-0.254**	**0.039**	**MT1**	**metallothionein 1F**
MT1G	**0.224**	**0.043**	**MT1, MT1K**	**metallothionein 1G**
GLRX3	**0.256**	**0.045**	**GLRX4, GRX3, GRX4, PICOT, TXNL2, TXNL3**	**glutaredoxin 3**
TXN*	**0.240**	**0.050**	**TRDX, TRX, TRX1**	**thioredoxin**
FTH1†	0.206	0.061	FHC, FTH, FTHL6, HFE5, PIG15, PLIF	ferritin heavy chain 1
GSR*	0.328	0.061	HEL-75, HEL-S-122m	glutathione-disulfide reductase
MSRA	-0.222	0.082	PMSR	methionine sulfoxide reductase A
TXNDC5	0.217	0.085	ENDOPDI, ERP46, HCC-2, HCC2, PDIA15, STRF8, UNQ364	thioredoxin domain containing 5
MT1M	-0.213	0.106	MT-1M, MT-IM, MT1, MT1K	metallothionein 1M
GPX7	0.210	0.110	CL683, GPX6, GPx-7, GSHPx-7, NPGPx	glutathione peroxidase 7
TXNRD2	-0.166	0.164	SELZ, TR, TR-BETA, TR3, TRXR2	thioredoxin reductase 2
ERP44	0.170	0.165	PDIA10, TXNDC4	endoplasmic reticulum protein 44
PRDX4	0.153	0.173	AOE37-2, AOE372, HEL-S-97n, PRX-4	peroxiredoxin 4
SOD2	0.191	0.238	IPO-B, IPOB, MNSOD, MVCD6, Mn-SOD	superoxide dismutase 2, mitochondrial
PDIA6	0.132	0.250	ERP5, P5, TXNDC7	protein disulfide isomerase family A member 6
TXNDC8	-0.176	0.262	SPTRX-3, TRX6, bA427L11.2	thioredoxin domain containing 8
GPX4	-0.125	0.315	GPx-4, GSHPx-4, MCSP, PHGPx, SMDS, snGPx, snPHGPx	glutathione peroxidase 4
SOD1	0.126	0.338	ALS, ALS1, HEL-S-44, IPOA, SOD, hSod1, homodimer	superoxide dismutase 1, soluble

Symbol	log_2 fold change	Adjusted *P* value	Synonyms	Description
TMX1	0.140	0.354	PDIA11, TMX, TXNDC, TXNDC1	thioredoxin related transmembrane protein 1
GLRX	-0.110	0.375	GRX, GRX1	glutaredoxin
TXNDC17	0.111	0.404	TRP14, TXNL5	thioredoxin domain containing 17
MT1A	-0.096	0.479	MT1, MT1S, MTC	metallothionein 1A
PRDX3	0.084	0.486	AOP-1, AOP1, HBC189, MER5, PRO1748, SP-22, prx-III	peroxiredoxin 3
GLRX2	0.086	0.500	CGI-133, GRX2	glutaredoxin 2
NME9	0.093	0.506	NM23-H9, TXL-2, TXL2, TXNDC6	NME/NM23 family member 9
TXNDC12	0.114	0.539	AG1, AGR1, ERP16, ERP18, ERP19, PDIA16, TLP19, hAG-1, hTLP19	thioredoxin domain containing 12
MT1X	0.104	0.544	MT-1I, MT1	metallothionein 1X
PRDX6	0.081	0.549	1-Cys, AOP2, HEL-S-128m, NSGPx, PRX, aiPLA2, p29	peroxiredoxin 6
GPX6	-0.087	0.567	GPX5p, GPXP3, GPx-6, GSHPx-6, dJ1186N24, dJ1186N24.1	glutathione peroxidase 6
GPX3	-0.073	0.622	GPx-P, GSHPx-3, GSHPx-P	glutathione peroxidase 3
TMX2	0.063	0.637	CGI-31, PDIA12, PIG26, TXNDC14	thioredoxin related transmembrane protein 2
CAT	0.068	0.642	-	catalase
PRDX5	-0.064	0.662	ACR1, AOEB166, B166, HEL-S-55, PLP, PMP20, PRDX6, PRXV, SBBI10, prx-V	peroxiredoxin 5
MT1E	-0.091	0.687	MT-1E, MT-IE, MT1, MTD	metallothionein 1E
GPX5	0.053	0.694	HEL-S-75p	glutathione peroxidase 5
GPX1	-0.059	0.698	GPXD, GSHPX1	glutathione peroxidase 1
SOD3	-0.048	0.763	EC-SOD	superoxide dismutase 3, extracellular
GLRX5	-0.047	0.777	C14orf87, FLB4739, GRX5, PR01238, PRO1238, PRSA, SIDBA3, SPAHGC	glutaredoxin 5
SELENOP	0.040	0.794	SELP, SEPP, SEPP1, SeP	selenoprotein P
TXN2	0.052	0.832	COXPD29, MT-TRX, MTRX, TRX2	thioredoxin 2
CCS	-0.031	0.841	-	copper chaperone for superoxide dismutase
MT1H	0.041	0.853	MT-0, MT-1H, MT-IH, MT1	metallothionein 1H
CP	0.023	0.889	CP-2	ceruloplasmin
TXNIP	0.151	0.899	ARRDC6, EST01027, HHCPA78, THIF, VDUP1	thioredoxin interacting protein
TXNDC11	-0.021	0.907	EFP1	thioredoxin domain containing 11
PRDX2	0.016	0.935	HEL-S-2a, NKEF-B, NKEFB, PRP, PRX2, PRXII, PTX1, TDPX1, TPX1, TSA	peroxiredoxin 2
MT2A	-0.014	0.942	MT2	metallothionein 2A
NME8	-0.015	0.943	CILD6, HEL-S-99, NM23-H8, SPTRX2, TXNDC3, sptrx-2	NME/NM23 family member 8
TXNDC2	-0.012	0.953	SPTRX, SPTRX1	thioredoxin domain containing 2

Symbol	log_2 fold change	Adjusted *P* value	Synonyms	Description
TMX4	-0.011	0.961	DJ971N18.2, PDIA14, TXNDC13	thioredoxin related transmembrane protein 4
MT1B	-0.009	0.963	MT-1B, MT-IB, MT1, MT1Q, MTP	metallothionein 1B
TXNL1	-0.013	0.968	HEL-S-114, TRP32, TXL-1, TXNL, Txl	thioredoxin like 1
GPX2	-0.008	0.969	GI-GPx, GPRP, GPRP-2, GPx-2, GPx-GI, GSHPX-GI, GSHPx-2	glutathione peroxidase 2
TMX3	-0.007	0.982	PDIA13, TXNDC10	thioredoxin related transmembrane protein 3

†Anti-oxidant genes identified from Enrichr search and Gorrini *et al.* (2013), and included in **Fig. 3a**.

*Anti-oxidant genes identified from Enrichr search, Gorrini *et al.* (2013) and Gelain *et al.* (2009), and included in **Fig. 3a**.